

Original Article

Cite this article: Ansari AH, Pandey SK, Ahmad S, Sharma M, Govil P, Chaddha AS, and Sharma A (2023) High primary productivity in an Ediacaran shallow marine basin influenced by strong seasonal to perennial upwelling. *Geological Magazine* **160**: 1607–1623. <https://doi.org/10.1017/S0016756823000614>

Received: 25 January 2023

Revised: 13 September 2023

Accepted: 18 September 2023

Keywords:

Late Neoproterozoic; Vindhyan Supergroup; Sirbu Shale; Palaeoproductivity; Palaeoredox; Cadmium; Upwelling

Corresponding author:

S.K. Pandey; Email: skpandey@bsip.res.in

High primary productivity in an Ediacaran shallow marine basin influenced by strong seasonal to perennial upwelling

A.H. Ansari, S.K. Pandey , Shamim Ahmad, Mukund Sharma, Pawan Govil, Amritpal Singh Chaddha and Anupam Sharma

Birbal Sahni Institute of Palaeosciences, Lucknow 226007, India

Abstract

A significant area of late Neoproterozoic–early Cambrian seafloor hosted a ferruginous to euxinic condition as a result of expanded primary productivity-driven pumping of organic matter into subsurface water column and weak water column mixing in the concomitant sea. However, the cause and extent of increased marine primary productivity during this time interval remain unknown. To estimate the primary productivity in a late Neoproterozoic sea, this study investigated the Sirbu Shale, Vindhyan Supergroup, for trace elements, organic carbon isotopes and total organic carbon (TOC). Among the trace elements, cadmium (Cd), known for extremely low concentration in crustal rocks but higher abundance in biogenic organic matter, was the key parameter in the palaeoproductivity estimation. The Cd enrichment in the Sirbu Shale samples is comparable to that in modern marine sediments of the oxygen minimum zones in Chilean margins, Arabian Sea and Gulf of California characterized by high primary productivity and seasonal upwelling. In terms of Cd enrichment, the lower section of the Sirbu Shale was deposited under suboxic conditions, while the upper section was deposited under a relatively less reducing condition. Cd/Mo ratios > 0.36 in the shale sample indicate that the palaeoproductivity was strongly influenced by the nutrient supply through sea-shelf upwelling. Using non-detrital enrichment of Cd in Sirbu Shale samples, we calculated that the TOC exported to the floor of Sirbu Shale palaeodepositional setting through primary productivity ranged from 0.71 to 10.16%.

1. Introduction

The rapid evolution of the Ediacaran biota and subsequent explosion and diversification of animals in the Ediacaran-early Cambrian is thought to have been driven by one of the most significant oxygenation events of the earth's history, commonly known as the Neoproterozoic Oxidation Event (NOE) (Xiao & Laflamme, 2009; Erwin *et al.* 2011; Knoll, 2011; Lenton *et al.* 2014). During the NOE, atmospheric oxygen concentration reached above 40% of the present atmospheric level and probably, for the first time, oxidized the deep oceanic floor (Canfield *et al.* 2007; Sahoo *et al.* 2012). This rise in oxygen level would have assisted the animal evolution, by developing more efficient metabolic machinery (Jiang *et al.* 2012), increasing the bioavailability of critical trace metals (Anbar & Knoll, 2002) and macronutrients. However, more recent studies have suggested that deep-water oxygenations between NOE and early Cambrian were transient, and deep-water column stayed anoxic to ferruginous for most of this interval, probably due to high surface primary productivity and associated dissolved oxygen consumption during organic matter remineralization (Li *et al.* 2015; Sahoo *et al.* 2016; Jin *et al.* 2016; Sperling *et al.* 2015). This theory of a drastic increase in primary productivity is supported by the rise in the abundance of phosphorites and phosphorus content in the geological records (Reinhard *et al.* 2017). However, for this period, oceanic primary productivity and its control (e.g., nutrient supply from terrestrial weathering or/and upwelling) remain poorly constrained (Xiang *et al.* 2018).

Redox shifts in oceanic bottom waters and sedimentary pore waters are often coupled with the change of the biological pump strength, a process through which inorganic dissolved carbon is fixed as organic matter by phytoplankton in the upper oceanic water column and subsequently exported to the deep ocean (Meyer *et al.* 2016). During this exportation, a significant fraction of organic matter is remineralized back to CO₂ by heterotrophs first consuming dissolved oxygen and thereafter other oxidants such as nitrate, manganese, iron and sulphate (Wyrteki, 1962). Thus, the degree of oxygen removal from the water column largely depends upon the strength of the biological pump or organic matter transfer into the water column. This process of dissolved oxygen removal from the water column directly/indirectly plays a key role in the accumulation of redox-sensitive trace elements (RSTEs) in underlying

© The Author(s), 2023. Published by Cambridge University Press. This is an Open Access article, distributed under the terms of the Creative Commons Attribution licence (<http://creativecommons.org/licenses/by/4.0/>), which permits unrestricted re-use, distribution and reproduction, provided the original article is properly cited.



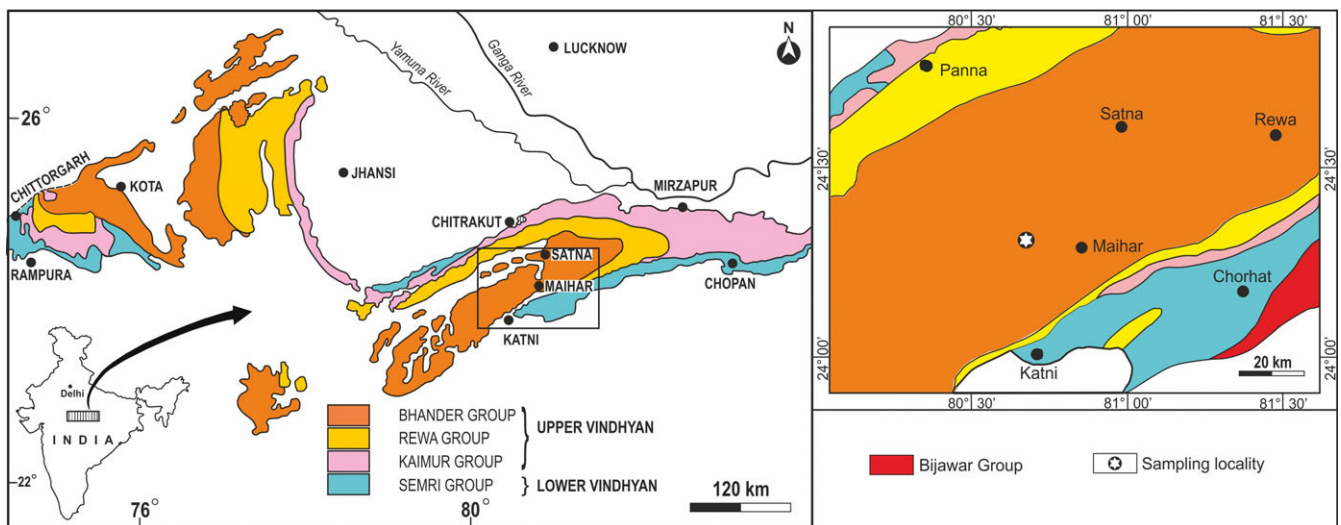


Fig. 1. (Colour online) Geological map of the Vindhyan Basin (after Krishnan & Swaminath, 1959) in and around Maihar area, Satna district. Star represents the sampling location of the Dudhiya Nala, North of Sharda Devi Temple, Maihar township.

sediments. It makes some of the biologically important RSTEs (Cd, Zn, Mo) a suitable proxy for understanding past export production (Wagner *et al.* 2013). Nevertheless, it is important to note that the remobilization of RSTEs during diagenetic processes can alter the sediment composition, rendering it challenging to use RSTEs for export production estimation. Besides, most of the available Proterozoic geological records are of shallow depositional origin that could have received detrital inputs from local specific mineral assemblages enriched or depleted in specific trace metals. This risk is minimal for elements that are low in crustal rocks but highly incorporated in biogenic particles (Brumsack, 2006). Cadmium (Cd) is one such RSTEs, the crustal abundance of which is very low but extensively accumulated in marine phytoplankton biomass (Rosenthal *et al.* 1995; Ho *et al.* 2003; Morel & Malcolm, 2005; Böning *et al.* 2005; Twining & Baines, 2013; Bryan *et al.* 2021). For example, Cd concentration in marine phytoplankton can reach up to more than two orders of magnitude compared to crustal abundance (Brumsack, 2006; Wagner *et al.* 2013).

Cadmium in the marine water column exhibits a nutrient-like profile, especially similar to dissolved inorganic phosphate, and it is effectively utilized by phytoplankton in the upper water column and released in the deeper water column during organic matter remineralization (Boyle *et al.* 1976; Cullen, 2006; Hendry *et al.* 2008). Though the role of phosphate as a bio-essential nutrient is well known, the role of Cd is still not properly understood. A few studies have reported Cd-based carbonic anhydrase enzyme, which plays a role in converting bicarbonate to carbon dioxide in photosynthetic CO₂ fixation (Lane *et al.* 2005; Xu *et al.* 2008). Furthermore, Cd assimilation in certain phytoplankton is higher under Zn/Fe-limited oceanic conditions (Cullen, 2006; Löscher *et al.* 1998; Price & Morel, 1990). The remarkable similarity of Cd distribution with the inorganic phosphate and organic carbon in modern Oceans has been proven useful in effectively reconstructing the palaeonutrient and palaeoproductivity from Cd concentration in clastic sediments (Brumsack, 2006; Wagner *et al.* 2013). More recently, novel Cd isotope studies on the Mesoproterozoic (Viehmann *et al.* 2019), Neoproterozoic to Cambrian (Hohl *et al.* 2017, 2019, 2020; John *et al.* 2017) and Permian (Georgiev *et al.* 2015) sedimentary rock records demonstrated that Cd is closely associated with biogenic organic matter and sulphide. Thus, to

develop a better understanding of the late Neoproterozoic palaeoproductivity and their controlling factors, this study investigated a section of the Ediacaran Sirbu Shale of the Vindhyan Supergroup, India, for trace elements and organic carbon isotopes analysis with special emphasis on the use of authigenic Cd as a palaeoproductivity proxy.

2. Geological background and age

The Vindhyan Supergroup (VSG) is one of the largest well-exposed intracratonic basins (Figure 1), occupying an area of about 1,66,400 km² in central and western India, with 40,000 km² under the subsurface profile of Deccan Trap and approximately 10,000 km² under the Gangetic alluvium (Srivastava *et al.* 1983; Mathur, 1987; Jokhan Ram *et al.* 1996; Sharma *et al.* 2020). In terms of thickness, age and depositional environment, the VSG is coeval to the other Proterozoic cratonic basins found in other parts of the world, such as America, Siberia, China and Australia (Preiss & Forbes, 1981; Deb, 2004; Wani & Mondal, 2011; Mahon *et al.* 2014; Rogov *et al.* 2015; Cawood *et al.* 2018; Rooney *et al.* 2018; Gladkochub *et al.* 2019). The basin unconformably rests on the top of the Bundelkhand massif (in the west and central parts) and the Bijawar Group of rocks (in the eastern part), which has been considerably metamorphosed (Crawford & Compston, 1969; Mondal *et al.* 2002). VSG is constituted of largely unmetamorphosed/undeformed rocks (Soni *et al.* 1987) and is exposed in two geographical locations: in central India (known as the Son Valley) and in western India (known as the Chambal Valley). The maximum cumulative thickness of the basin is around 5000 metres, composed of mainly sandstone, shale, limestone and, to a lesser extent, mudstone, siltstone, porcellanite and ash beds (Bhattacharyya, 1993, 1996). It is broadly divided into lower and upper Vindhyan. The entire succession is lithostratigraphically divided into four groups, viz. the Semri, the Kaimur, the Rewa and the Bhandar, in ascending order (Table 1). The Bhandar Group, the youngest unit (Krishnan, 1968; Sastry & Moitra, 1984), is composed of shale-carbonate-shale-sandstone litho-package and subdivided into four formations: the Ganurgarh Shale, the Bhandar Limestone, the Sirbu Shale and the Maihar Sandstone (Table 1).

Table 1. Lithostratigraphy of the Vindhyan Supergroup (modified after Sastry & Moitra, 1984; Kumar & Sharma, 2012; Sharma *et al.* 2020)

Age	VINDHYAN SUPERGROUP	Group	Formation	Lithology	Significant fossil	Geochronology
Neoproterozoic		Bhandar	Maihar Sandstone	Sandstone, siltstone	Ediacaran age: <i>Arumberia banksi</i> , <i>A. vindhyanensis</i> , <i>Rameshia rampurensis</i> and <i>Beltanelliformis minuta</i> (Kumar & Pandey, 2008) <i>Charniodiscus</i> -like Ediacaran megafossil (Pandey <i>et al.</i> 2023b)	< 548 Ma (Lan <i>et al.</i> 2020) U-Pb < 770 Ma (Kumari <i>et al.</i> 2023) U-Pb ≤ 1000 Ma (McKenzie <i>et al.</i> 2011) U-Pb ~1020 Ma (Malone <i>et al.</i> 2008) U-Pb
			Sirbu Shale	Shale, siltstone	Ediacaran age: <i>Obruchevella parva</i> , <i>O. valdaica</i> , <i>O. parvissima</i> , <i>O. blandita</i> , <i>O. delica</i> (Prasad, 2007; Prasad <i>et al.</i> 2005); Late Ediacaran Leiosphere Palynoflora (LELP) assemblage (Pandey <i>et al.</i> 2023b)	741 ± 9 Ma (Rathore <i>et al.</i> 1999) K-Ar
			Bhandar Limestone	Limestone, shale	Stromatolites (Kumar, 1976a, b; Misra & Kumar, 2005) Ediacaran age: <i>Obruchevella parva</i> , <i>O. valdaica</i> , <i>O. parvissima</i> , <i>O. blandita</i> , <i>O. delica</i> (Prasad, 2007; Prasad <i>et al.</i> 2005); Organic-walled microfossils (OWMs) (Singh <i>et al.</i> 2011; Pandey & Kumar, 2013); Sponge spicule-like forms (Kumar, 1999); Ediacaran Vase-shaped like microfossils (VSMs) (Pandey <i>et al.</i> 2023b)	908 ± 72 Ma (Gopalan <i>et al.</i> 2013) Pb/Pb
			Ganurgarh Shale	Shale, calcareous siltstone	<i>Obruchevella parva</i> , <i>O. valdaica</i> , <i>O. parvissima</i> , <i>O. blandita</i> , <i>O. delica</i> (Prasad, 2007; Prasad <i>et al.</i> 2005): preservation not good.	–
		Rewa	Upper Rewa Sandstone	Sandstone	Devoid of fossil	–
			Jhiri Shale	Shale, fine sandstone	<i>Chuarina-Tawuia</i> Assemblage (Rai <i>et al.</i> 1997)	–
			Lower Rewa Sandstone	Sandstone, siltstone	Devoid of fossil	–
			Panna Shale	Shale	<i>Chuarina-Tawuia</i> Assemblage (Srivastava, 2004)	–
Upper Mesoproterozoic		Kaimur	Dhandraul Quartzite	Quartzite	Devoid of fossil	–
			Mangesar Formation	Sandstone and shale	Devoid of fossil	–
			Bijaigarh Shale	Black shale	Microbial Mats (Sur <i>et al.</i> 2006)	1210 ± 22 Ma (Tripathy & Singh, 2015) Re-Os
			Ghaghar Sandstone	Sandstone and shale	Devoid of fossil	–
			Susnai Breccia	Brecciated sediments	Devoid of fossil	–
			Sasaram Formation	Sandstone and mudstone	Devoid of fossil	–
Upper Palaeo - Lower Mesoproterozoic		Semri	Limestone, dolostone, shale, sandstone, porcellanite	Fossils (see Sharma <i>et al.</i> 2020 and reference therein)	Geochronological ages (see Table 8 in Sharma <i>et al.</i> 2020)	
Unconformity						
Mahakoshal, Aravalli, Bundelkhand Granite						

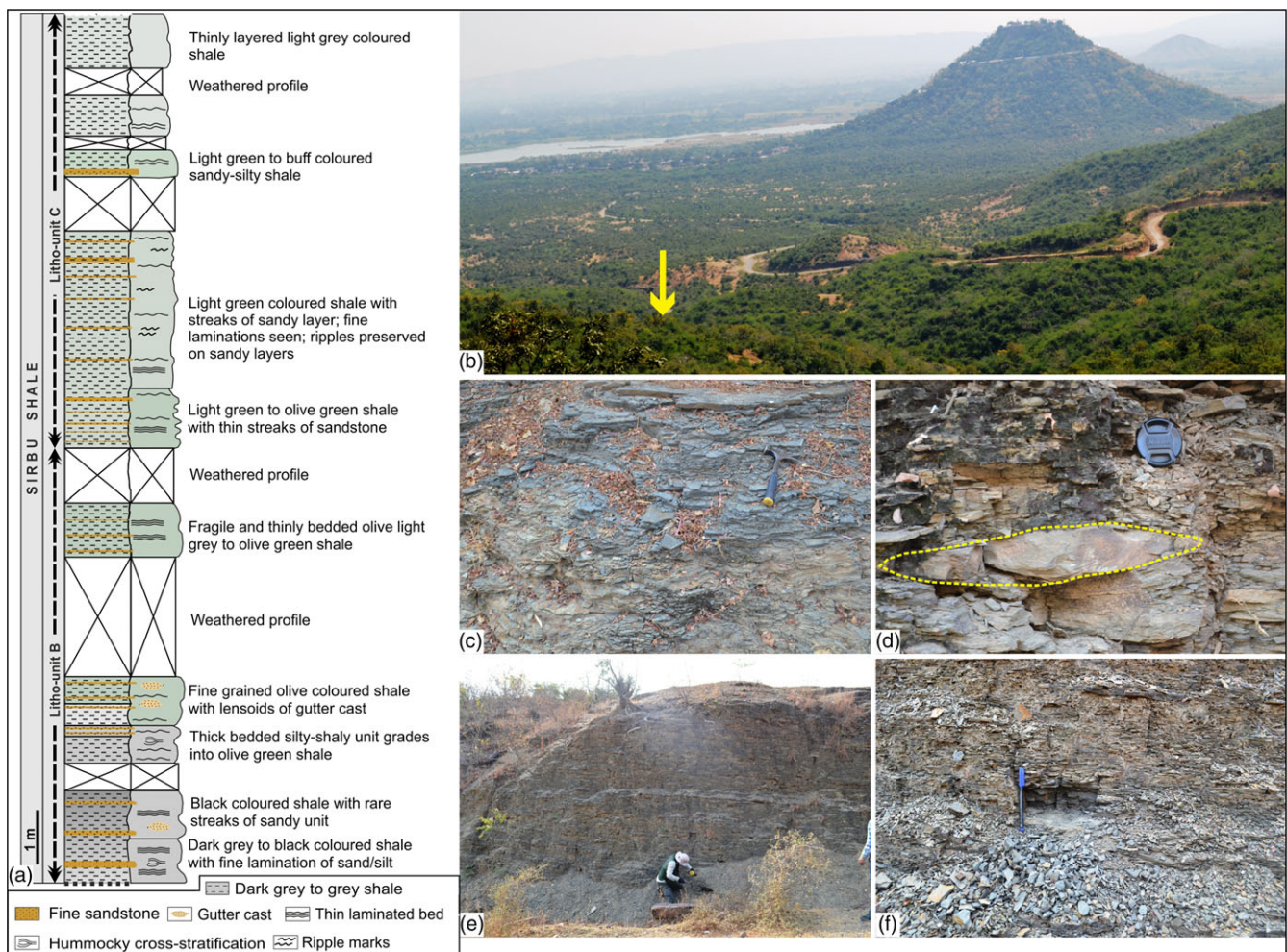


Fig. 2. (Colour online) (a) Detailed litholog of the Sirbu Shale exposed in Dudhiya Nala Section; (b) Dudhiya Nala section, where thin layers of black to grey-coloured shale/mudstone/sandy unit of the Sirbu Shale is exposed (see yellow arrow); (c) Litho-unit B of the Sirbu Shale: papery thin green, dark grey to black coloured shale with intercalations of centimetric thin sandy layers; (d) lensoid sandy gutter cast (yellow dotted line) indicates small events of storms within Litho-unit B; (e), (f) partly sandy and light grey to green colour shale in the middle and buff colour at the top.

The Ganurgarh Shale is an older unit of the Bhandar Group characterized by maroon colour fine-grained calcareous silty shale. A few outcrop exposures are available around Rewa and Maihar area, Madhya Pradesh. The presence of salt pseudomorph and gypsum suggests that the Ganurgarh Shale was deposited in the upper intertidal to supratidal depositional setting (Singh, 1976; Sarkar *et al.* 2002). The overlying unit, the Bhandar Limestone, is exposed in the low-lying areas or mine or quarry sections in the Satna district. It is composed of dark grey-coloured carbonate with subordinate green to buff-coloured shale. Stromatolites are preserved as bioherms and biostromes in the Satna-Maihar area (Kumar, 1976a, b; Misra and Kumar, 2005; Pandey, 2012). Flaser and lenticular bedding, intraformational conglomerate, small-scale-cross bedding, fractured microbial layers, ripples and mud cracks are some of the sedimentary structures profusely developed within the carbonate units. The lowest part of this carbonate unit was deposited in moderate energy, subtidal to lower intertidal depositional setting. In contrast, the middle to upper part was deposited in an intertidal to supratidal depositional setting (Singh, 1976).

The Sirbu Shale is well exposed in hillock sections in and around the Maihar area with overlying Maihar Sandstone and

underlying Bhandar Limestone (Figure 1, 2) and composed of light yellow-buff, grey to greyish green shale and siltstone interbedded with grey to brownish grey mudstone siltstone and sandstone suitable facies for fossil preservation. The estimated thickness of the Sirbu Shale is 100–250 m (Sastry & Moitra, 1984). Based on the sedimentological variations, Singh (1976) divided it into three litho-units: litho-unit A, B and C in ascending order and inferred to be deposited in a lagoon with oxidizing milieu, hypersaline and storm-dominated palaeoenvironment. Sarkar *et al.* (2002) inferred it to be deposited in storm-dominated shelf and lagoonal palaeoenvironment. A recent study by Singh and Chakraborty (2022) suggested that the Sirbu Shale is deposited within the storm-dominated outer to inner shelf towards the top based on the physical evidence. In the present study, the classification given by Singh (1976) is being followed for the ease of understanding the different litho-units. Litho-unit A is composed of dark brown to maroon-coloured sand-siltstone with occasional layers of green-coloured shale. Various types of shallow water ripple marks are well exposed, along with intermittent sub-areal exposure. It was deposited in the protected mudflat to the lagoonal hypersaline environment as indicated by the presence of salt-pseudomorphs. It is not exposed in the studied section of Dudhiya nala. Litho-unit B

is characterized by the papery thin green, dark grey to black coloured shale (Figure 2(a), (c)) with intercalations of centimetric thin sandy layers (Figure 2(a), (c)) at about 1-metre intervals. Fresh cuttings are typically dark grey in colour, but when exposed to light, they turn brown. Gutter cast, hummocky cross-stratification and load cast are common sedimentary structures between the shaley layers of this unit, suggesting storm-dominated events within the depositional realm (Figure 2(a), (d)). Thus, this unit is inferred to be deposited above the storm wave base or in storm-dominated shelf palaeoenvironment (Singh, 1976; Sarkar *et al.* 2002). Litho-unit C comprises decimetre thick sandy layers interbedded with reddish-brown shale, but in fresh cut, light green in the middle and light grey at the top (Figure 2(a), (e), (f)).

Both the litho-units B and C are quite different in terms of grain texture, lithology, colour and deposition environment. Litho-unit B is papery thin with the lower part dark grey to grey and the upper part light green in colour. Litho-unit C is light grey in the lower part and light grey at the top (Figure 2(f)) composed of coarse and thickly bedded shale with intercalation of centimetre size sandy layer (Sarkar *et al.* 2002). The litho-unit B is dominated by the gutter cast, whereas in litho-unit C, its presence is rare. The change from litho-unit B to C symbolises a shift in depositional setting from a relatively deeper shelf to a relatively shallower shelf environment (Sarkar *et al.* 2002).

The Maihar Sandstone, characterized by heterolithic stratification of sandstone and siltstone, has a gradational contact with the underlying Sirbu Shale and is best exposed in Maihar township. Cross stratifications, flaser, lenticular bedding, desiccation cracks, penecontemporaneous deformational structures, wave, current ripples and many other sedimentary structures are well preserved within the Maihar Sandstone. The Maihar Sandstone is deposited in the tidal flat–shoal complex depositional environment (Singh, 1976).

The Ganurgarh Shale represents the base of the Bhandar Group. Prasad *et al.* (2005) and Prasad (2007) recovered organic-walled microfossil assemblages from subsurface profile (core) and outcrop sections and suggested the late Cryogenian to early Vendian age. From the overlying Bhandar Limestone, Kumar (1999) reported sponge spicule-like structure, and Singh *et al.* (2011) and Pandey & Kumar (2013) reported microfossils assemblage from the associated black bedded chert and suggested Ediacaran age. Columnar stromatolites and carbonaceous megafossils were reported from the Bhandar Limestone (Valdiya, 1969; Kumar, 1976a, b; Kumar & Srivastava, 1997, 2003; Misra & Kumar, 2005; Singh *et al.* 2009; Sharma *et al.* 2009; Pandey, 2012). Pandey *et al.* (2023b) described large-sized Ediacaran Vase-shaped microfossils (VSMs) from the Bhandar Limestone. The Bhandar Limestone is overlain by the Sirbu Shale, from where Kumar & Srivastava (2003) have described *Chuararia-Tawuia* and other carbonaceous assemblage and suggested the upper Riphean and Vendian age of the Bhandar Group. A variety of the Ediacaran-type megafossils were reported from the different shale units of the Sirbu Shale (De, 2003, 2006, 2009), yet their biogenicity is not proven. Recently, Pandey *et al.* (2023b) described Ediacaran 'Late Ediacaran Leiosphere Palynoflora' (LELP) assemblage and other associated organic-walled microfossils from the Sirbu Shale. The Ediacaran fossils, such as *Arumberia banksi* (Vendobionta), *A. vindhyanensis*, *Rameshia rampurensis*, *Beltaneliformis minuta*, *Dickinsonia tenuis* (?) and *Charniodiscus*-like Ediacaran megafossil have been reported and discussed from the Maihar Sandstone and considered to be deposited within the late Ediacaran Period (Kumar & Pandey, 2008; Pandey, 2012; Retallack *et al.* 2021;

Pandey *et al.* 2023b). However, *Dickinsonia tenuis* has been challenged by Pandey *et al.* (2023a) and Meert *et al.* (2023) and proven to be a pseudofossil.

Stable carbon isotope studies on the Bhandar Limestone and carbonate lenses of the Sirbu Shale suggested a probable Precambrian-Cambrian boundary between the Bhandar Limestone and the Sirbu Shale (Friedman *et al.* 1996; Friedman & Chakraborty, 1997) though only few samples have been analyzed. Stable carbon and strontium isotope analyses of the Bhandar Limestone by Ray *et al.* (2002, 2003); Kumar *et al.* (2002); and Kumar *et al.* (2005) suggested Tonian to Cryogenian (~750–650 Ma) age. Rathore *et al.* (1999) dated glauconites occurring in the lowest part of the Sirbu Shale by the K-Ar method and gave 741 ± 9 Ma age for deposition of the Sirbu Shale. Recently, Lan *et al.* (2020) dated the topmost unit of the Maihar Sandstone by the U-Pb method, and based on the youngest zircon dataset, the maximum depositional age was estimated as 548 Ma. Lan *et al.* (2020) dataset matches the overall fossil assemblage recovered from the Maihar Sandstone. Recent and previous reports of the Ediacaran elements (fossils and radiometric ages) from the Maihar Sandstone (Kumar & Pandey, 2008; McKenzie *et al.* 2011; Lan *et al.* 2020; Retallack *et al.* 2021; Pandey *et al.* 2023b) stress the plausible Ediacaran age of the Sirbu Shale.

3. Materials and methods

This study was performed on the uppermost succession of litho-units B and C, which is best exposed (about 16 m) in the Dudhiya Nala section, North of Sharda Devi temple on Maihar to Rampur Road (Figure 2(a), (b)). For the geochemical investigation, 48 samples were systematically collected (24°16'32.00" N; 80°43'10.00" E) (Figure 1, 2). Each sample's surface was discarded, and the remainder part was washed thrice with Milli-Q water and dried at 60°C in the oven. Samples were powdered for the geochemical analysis. Entire preprocessing was performed at the Birbal Sahni Institute of Palaeosciences (BSIP), Lucknow.

Thirty mg powder of each sample was digested in the two-step process for trace element analyses (Xiong *et al.* 2012; Ansari *et al.* 2020, 2022). In the first step, the powdered sample was transferred into a Teflon tube and added with a 5 mL mixture of hydrofluoric and nitric acid in a 2:1 ratio followed by 1 mL perchloric acid. Subsequently, the tube was tightly closed with a cap and heated at 120°C for 7 hours in a Q-block operating system. Later, the Teflon tube was opened to allow the evaporation until it dried completely. In the second step, a 5 mL mixture of hydrofluoric acid and nitric acid in a 1:2 ratio followed by 1 mL of perchloric acid was added into the Teflon tube, then heated and dried as in the first step. After the second step, 2 mL of 5% HNO₃ was added, and the clarity of the solution was checked. If any part of the powdered sample was still left, the two-step process was repeated until complete digestion. The digested sample was diluted in 2% HNO₃ to a final volume of 50 mL and kept at 4°C before analysis. Similarly, the digested liquid was prepared from United States Geological Survey (USGS) standard rock powders of Cody Shale (SCo-1), Green River Shale (SGR-1b), and blanks. Repeats of some samples were run for quality control. The analytical error was less than 5%.

The $\delta^{13}\text{C}$ -org and TOC analysis was carried out following the method described by Ansari *et al.* (2018). The powdered sample was first treated with 5% HCl to remove traces of carbonates. The treated sample was washed with Milli-Q water and then dried at 60°C in the oven. The dried sample was again crushed to powder, weighted and enclosed in a tin capsule, which was inserted into a

prefilled, conditioned reactor of the Elemental Analyser (Flash EA 2000 HT) by the integrated autosampler. For isotopic analysis, the CO₂ released from the combustion of the sample in EA was transferred to the Isotope Ratio Mass Spectrometer (IRMS MAT 253) coupled with the Con-Flow IV interface. To check the accuracy of isotopic measurements, international standards: IAEA-CH3 and IAEA-CH6, internal standards: Sulfanilamide and a few repeat samples were repeatedly analyzed at the interval of ten samples. TOC was measured from the peak area of CO₂ chromatogram from mass spectrometer (Agrawal *et al.* 2015).

For quantitative elemental analyses, a wavelength Dispersive X-Ray Fluorescence (WD-XRF) Spectrometer (Model: PANalytical, Axios max, 4 KW) was used. Samples were ground into powder using an agate mortar and pestle (up to around 300 mesh of ASTM standard). The powdered specimens were then moulded into pressed pellets in a ratio of 6:4 (sample: binder) using boric acid as a binder, following the method described by Takahashi (2015). The individual samples were examined using the international standards and a Super Q application with an accuracy of ≤5%. All these analyses were performed at the Sophisticated Analytical Instrument Facilities (SAIF) of the BSIP. Repeat analyses showed a precision of ±0.1%. Loss on ignition (LOI), which reflects the volatile content in the samples, was measured by heating the 5 g of the sample at 950°C for 6 hours in a muffle furnace and subtracting the final weight of the sample from 5 g (weight before heating).

3.1. Calculation of enrichment factors for elements

To understand the relative enrichments of trace elements in the bulk samples of Sirbu Shale against the average composition of upper continental crust (UCC) (Rudnick & Gao, 2003), the enrichment factor (EF) for trace element is calculated using following Eq. 1.

$$X_{EF} = (X/Al)_{\text{sample}} / (X/Al)_{\text{UCC}} \quad (1)$$

X and EF in Eq.1 represent trace element and enrichment factors, respectively. 'Al' represents element aluminium. (X/Al)_{sample} and (X/Al)_{UCC} denote the ratio in the bulk samples of Sirbu Shale and the ratio for the average composition of UCC. Al in Eq. 1-4 is used as a tracer for calculating the detrital fraction of trace elements. An example of enrichment factor calculation is provided in the Supplementary Material (after supplementary Table 2).

3.2. Calculation of TOC_{bm} and TOC_{loss}

Studies of the Cd content in surface marine sediments and phytoplankton of modern ocean (Rosenthal *et al.* 1995; Ho *et al.* 2003; Morel & Malcolm *et al.* 2005; Böning *et al.* 2005; Twining & Baines, 2013; Bryan *et al.* 2021) have demonstrated that Cd is strongly correlated with organic content and 1% of TOC generally contributes 0.186 to 0.372 µg of biogenic (non-detrital) Cd in modern marine sediments. This quantitative relation between TOC and non-detrital Cd thus can be used in estimating the possible range of TOC content in marine sediment records. Assuming that the quantitative transfer of non-detrital Cd to sediments in non-euxinic set-up of ancient ocean was also mainly driven by organic matter transport and in the similar ratio as in the modern ocean, we propose an equation (Eq.4) for the tentative estimation of total organic carbon originally exported to the concomitant sediment [i.e., TOC content in sediment before

reminereralization (TOC_{bm}) by early diagenetic activities] of ancient marine set-up.

$$Cd_{\text{non-detrital}} = Cd_{\text{sample}} - Cd_{\text{detrital}} \quad (2)$$

$$Cd_{\text{detrital}} = (Cd_{\text{UCC}}/Al_{\text{UCC}}) * Al_{\text{sample}} \quad (3)$$

$$TOC_{\text{bm}}(\%) = [Cd_{\text{sample}} - (Cd_{\text{UCC}}/Al_{\text{UCC}}) * Al_{\text{sample}}] / CF \quad (4)$$

In Eq. 4, CF is a conversion factor representing the quantitative relation between TOC and non-detrital Cd contributed in modern marine sediments that range from 0.186 to 0.372 (Rosenthal *et al.* 1995; Ho *et al.* 2003; Morel & Malcolm *et al.* 2005; Böning *et al.* 2005; Twining & Baines, 2013; Bryan *et al.* 2021). TOC_{bm} denotes the estimated gross organic matter export, i.e., TOC before loss through remineralization at the sediment-water interface or during early diagenesis. The remineralization loss of organic carbon (TOC_{loss}) is calculated by subtracting the TOC measured in the bulk sample from TOC_{bm} calculated for the respective sample (see Eq. 5).

$$TOC_{\text{loss}}(\%) = TOC_{\text{bm}} - TOC(\text{bulk}) \quad (5)$$

4. Results

A total of 48 shale samples collected from the Sirbu Shale were analyzed for trace metals, TOC, and bulk organic carbon isotope. However, 46 samples were analyzed for the major oxides and LOI as two samples (BH-29 and BH-35) were completely consumed and were unavailable for these analyses. Data have been provided in Tables 2a and 3, and supplementary Tables 1, 2 and 3. The correlation matrix among the enrichment factors of trace elements, total phosphorus (P) enrichment, Al, TOC, δ¹³C-organic, and LOI are given in Table 2b. The results show that only Cd is significantly enriched in the samples. The calculated enrichment factor using Eq.1 against the UCC values (Rudnick & Gao, 2003) for Cd in the litho-unit B (BH-1 to BH-24) varies between 7.1 and 28.5, and in the litho-unit C (BH-25 to BH-48) varies between 4.7 and 8.5 (Figure 3 and Supplementary Table 2). Enrichment of total P in litho-unit B varies between 1.6 and 3.2, and in the litho-unit C varies between 1.4 and 2.2. V and Cr enrichment factors in the sampled stratigraphic section show no significant change and stay consistent < 1 (Figure 3). Enrichment factor for Co and Mo in the litho-unit C and upper part of the litho-unit B does not show major changes and value mostly falls close to one, but the lower part of litho-unit B shows relatively significant enrichment (2–3 times) compared to UCC (Figure 3). Enrichment factor for U in litho-unit C and upper part of litho-unit B demonstrates a value consistently close to two and show a small stable rise up to a value around three in the lower part of litho-unit B (Figure 3). Total organic carbon and δ¹³C-org in the samples range from 0.06 to 0.26 weight% and from –22 to –26 ‰ respectively (Table 2a). The Cd_{EF} shows a weak but statistically significant (Pearson coefficient correlation < 0.05) negative correlation with δ¹³C-org and Al (Figure 4(c), (e) and Table 2b) and a statistically significant weak to moderate positive correlation with Co_{EF}, P_{EF} and Mn/Al (Figure 4(d) and Figure 5(a), (b)). The δ¹³C-org shows a weak but statistically significant positive correlation with TOC and LOI (Figure 4(a), (b) and Table 2b).

The minimum and maximum range for TOC_{bm} estimated by using Eq.4 are 0.71 to 5.08% (average 1.65%) and 1.43 to 10.16%

Table 2a. Trace elements (in ppm), Al, TOC, LOI (loss on ignition) (Weight%) and $\delta^{13}\text{C}$ -org (in ‰) data from the Sirbu Shale samples. BM denotes before remineralization and loss denotes loss during diagenesis of Sirbu Shale

Sample ID	V	Cr	Co	Ni	Mo	Cd	U	Mn	Al	LOI	TOC	$\delta^{13}\text{C}$
	$\mu\text{g/g (ppm)}$								Weight%			‰
BH-1	100	78	75	37	1.6	0.9	4.7	464.7	6.7	3.8	0.18	-26.4
BH-2	78	61	40	26	1.1	1.2	5.1	542.2	6.1	3.3	0.12	-26.0
BH-3	81	61	43	21	1.0	0.9	4.6	387.3	5.8	3.1	0.12	-25.4
BH-4	105	82	34	31	1.0	1.0	5.4	464.7	6.8	4.1	0.13	-26.0
BH-5	114	91	48	29	1.1	1.1	6.0	464.7	7.4	4.1	0.16	-25.0
BH-6	158	121	20	36	0.8	0.8	8.4	464.7	9.5	5.1	0.21	-24.9
BH-7	99	72	46	32	1.2	0.8	4.9	697.1	6.4	3.8	0.09	-24.8
BH-8	112	86	38	34	2.0	2.0	5.4	542.2	7.1	4.0	0.11	-24.6
BH-9	108	87	35	35	0.8	0.9	5.3	464.7	7.6	4.3	0.13	-24.5
BH-10	62	52	67	38	1.1	1.5	4.4	619.6	5.9	3.8	0.12	-25.6
BH-11	144	112	35	46	0.4	0.6	6.5	387.3	8.9	5.7	0.12	-24.8
BH-12	100	83	31	31	0.4	0.9	6.5	387.3	6.9	4.2	0.10	-24.1
BH-13	91	70	38	25	0.9	1.1	5.7	387.3	6.3	4.0	0.08	-24.8
BH-14	94	81	32	36	0.9	0.8	6.0	387.3	7.5	4.8	0.12	-24.5
BH-15	115	83	29	32	0.9	0.7	5.3	387.3	7.5	4.7	0.07	-24.9
BH-16	123	95	24	36	1.0	1.0	5.8	387.3	7.9	5.2	0.06	-25.8
BH-17	89	65	28	27	1.0	0.7	4.8	387.3	7.1	4.0	0.14	-23.6
BH-18	135	103	18	41	2.2	0.8	6.1	387.3	8.5	5.8	0.20	-24.0
BH-19	148	110	20	57	1.5	0.9	6.9	387.3	8.8	6.0	0.18	-24.4
BH-20	98	75	33	31	0.9	0.9	5.2	387.3	7.0	4.6	0.09	-24.3
BH-21	138	103	20	52	1.4	0.8	6.7	387.3	8.6	6.0	0.18	-23.4
BH-22	75	53	31	26	0.8	0.7	4.6	387.3	6.3	3.8	0.09	-24.4
BH-23	133	98	21	36	0.9	0.8	7.3	387.3	8.8	6.0	0.17	-24.4
BH-24	134	100	19	54	1.0	0.9	6.5	387.3	8.5	6.1	0.18	-23.8
BH-25	104	80	23	34	0.9	0.4	5.3	387.3	7.6	4.8	0.14	-24.2
BH-26	131	96	48	44	0.5	0.4	5.9	387.3	8.2	5.4	0.16	-23.8
BH-27	147	111	24	45	0.8	0.4	6.8	387.3	9.0	6.0	0.18	-23.7
BH-28	130	100	26	48	0.7	0.4	6.4	387.3	7.9	5.5	0.21	-23.5
BH-29	113	89	26	42	0.9	0.4	5.9	n.a.	n.a.	n.a.	0.16	-23.9
BH-30	124	98	26	24	1.1	0.5	7.3	387.3	9.8	5.0	0.21	-24.9
BH-31	128	100	35	35	0.6	0.5	6.6	387.3	8.1	4.9	0.18	-22.1
BH-32	122	96	28	38	0.9	0.7	6.0	464.7	8.0	5.3	0.26	-23.0
BH-33	122	90	17	37	0.4	0.5	5.8	387.3	7.9	5.1	0.18	-22.9
BH-34	122	114	22	47	1.2	0.5	6.0	387.3	7.8	5.5	0.22	-23.8
BH-35	100	103	26	46	1.9	0.4	4.6	n.a.	n.a.	n.a.	0.17	-23.8
BH-36	145	138	50	78	1.4	0.5	6.1	387.3	8.8	5.9	0.22	-24.8
BH-37	134	126	19	51	1.5	0.4	6.8	387.3	8.5	5.6	0.17	-23.0
BH-38	134	126	20	51	1.0	0.4	6.8	387.3	8.6	5.7	0.17	-23.3
BH-39	135	127	23	55	1.7	0.4	6.4	387.3	8.5	5.7	0.17	-23.0
BH-40	125	118	21	48	1.1	0.5	6.3	387.3	8.1	5.5	0.22	-24.1
BH-41	137	126	22	47	1.0	0.5	6.6	387.3	8.2	5.7	0.23	-22.7

(Continued)

Table 2a. (Continued)

Sample ID	V	Cr	Co	Ni	Mo	Cd	U	Mn	Al	LOI	TOC	$\delta^{13}\text{C}$
$\mu\text{g/g (ppm)}$									Weight%		‰	
BH-42	134	138	23	58	1.9	0.5	6.0	387.3	8.3	5.7	0.20	-22.9
BH-43	95	101	35	42	0.4	0.4	4.1	387.3	6.7	4.1	0.09	-24.1
BH-44	97	101	31	42	0.5	0.3	4.8	387.3	7.0	4.4	0.11	-23.2
BH-45	120	121	51	53	0.7	0.4	5.7	387.3	7.7	5.3	0.16	-23.8
BH-46	144	145	20	54	1.0	0.5	5.4	387.3	8.0	5.6	0.19	-23.2
BH-47	133	128	22	54	1.1	0.4	6.1	387.3	8.3	5.5	0.17	-22.8
BH-48	129	124	22	49	0.6	0.4	6.9	387.3	8.1	5.3	0.11	-25.4

Table 2b. Correlation matrix (R values) among trace elements enrichment factor, Al, Mn/Al, Fe/Al, TOC, $\delta^{13}\text{C}$ -org and LOI of Sirbu Shale samples

	V_{EF}	Cr_{EF}	Co_{EF}	Ni_{EF}	Mo_{EF}	Cd_{EF}	P_{EF}	Al	Mn/Al	Fe/Al	TOC	$\delta^{13}\text{C}$	LOI
V_{EF}	1.000												
Cr_{EF}	0.684	1.000											
Co_{EF}	-0.480	-0.350	1.000										
Ni_{EF}	0.411	0.712	-0.034	1.000									
Mo_{EF}	-0.038	-0.051	0.255	0.109	1.000								
Cd_{EF}	-0.422	-0.550	0.596	-0.330	0.504	1.000							
P_{EF}	-0.348	-0.339	0.459	-0.330	0.056	0.504	1.000						
Al	0.582	0.399	-0.719	0.196	-0.202	-0.640	-0.549	1.000					
Mn/Al	-0.473	-0.420	0.746	-0.156	0.368	0.738	0.594	-0.770	1.000				
Fe/Al	0.119	0.004	0.256	0.166	0.196	0.322	0.306	-0.550	0.505	1.000			
TOC	0.454	0.397	-0.354	0.310	0.065	-0.474	-0.347	0.617	-0.436	-0.401	1.000		
$\delta^{13}\text{C}$	0.351	0.447	-0.559	0.299	-0.230	-0.589	-0.394	0.394	-0.487	-0.040	0.452	1.000	
LOI	0.658	0.533	-0.715	0.495	-0.166	-0.663	-0.664	0.872	-0.749	-0.297	0.608	0.533	1.000

(average 3.31%), respectively (Figure 3 and Supplementary Table 3). The minimum and maximum range for TOC_{loss} estimated by using Eq.5 are 1.37 to 9.90% (average 3.16%) and 0.65 to 4.82% (average 1.5%), respectively (Supplementary Table 3). Stratigraphic variations in TOC_{bm} shows two distinct regimes: first covers the litho-unit B, in which average TOC_{bm} ranges from 2.33% to 4.66% (Figure 3 and Supplementary Table 3), and second the litho-unit C, in which average TOC_{bm} ranges from 0.98% to 1.96%. The average Cd/Mo ratio in litho-units B and C are 0.97 and 0.55.

5. Discussions

5.1. Diagenetic changes in Cd and $\delta^{13}\text{C}$ -org records

Prior understanding of diagenetic changes in the biogeochemical records of geologically aged sediments and rock samples is essential before those parameters can be used for palaeo-reconstructions. Early diagenetic processes in the sediments can remobilise the trace elements resulting in depletion or authigenic enrichment of the elements, which is commonly associated with aerobic and anaerobic oxidation of organic matter. These changes complicate the use of trace metals and stable isotopes for palaeo-reconstruction. In marine sediments, Cd buildup is frequently

observed in the suboxic to sulphidic zones in conjunction with organic matter and sulphides (Rosenthal *et al.* 1995). The oxidation of sedimentary sulphides and organic matter at the interface between oxic and anoxic horizons can fluctuate on a millimetre-scale within the top sediment depending on the bottom water oxygen condition. This process can remobilise some proportion of sedimentary Cd into the bottom water (Gendron *et al.* 1986; Rosenthal *et al.* 1995; van Geen *et al.* 1995). According to Rosenthal *et al.* (1995), Cd in sedimentary pore waters is primarily sourced from early diagenetic oxidation of sedimentary organic matter. It typically moves downward along the concentration gradients established by its removal near the redox boundary. The major removal of Cd from sedimentary pore waters may occur through the formation of insoluble CdS phases (Rosenthal *et al.* 1995; Plass *et al.* 2020) and to some extent by its adsorption on Fe/Mn oxide particles (McCorkle & Klinkhammer, 1991). According to Plass *et al.* (2020), the solubility of trace metals sulphides ($\text{CdS} \ll \text{FeS}/\text{FeS}_2$) is the crucial factor influencing their precipitation and accumulation in marine sediments. For example, CdS solubility in suboxic to anoxic conditions is found very low (Bryan *et al.* 2021; Chen *et al.* 2021; Janssen *et al.* 2014, 2019), but re-dissolution has been observed in highly sulphidic environments through formation of bi-sulphide

Table 3. The range of Th/Co and Th/Cr ratios in Sirbu Shale, felsic rocks, mafic rocks and upper continental crust

Elemental ratio	Sirbu Shale (This study)	Felsic Rocks (Cullers, 1994, 2000)	Mafic Rocks (Cullers, 1994, 2000)	Upper Continental Crust (UCC) (Rudnick and Gao, 2003)
Th/Co	0.26–1.63	0.67–19.40	0.04–1.40	0.61
Th/Cr	0.18–0.38	0.13–2.70	0.02–0.05	0.11

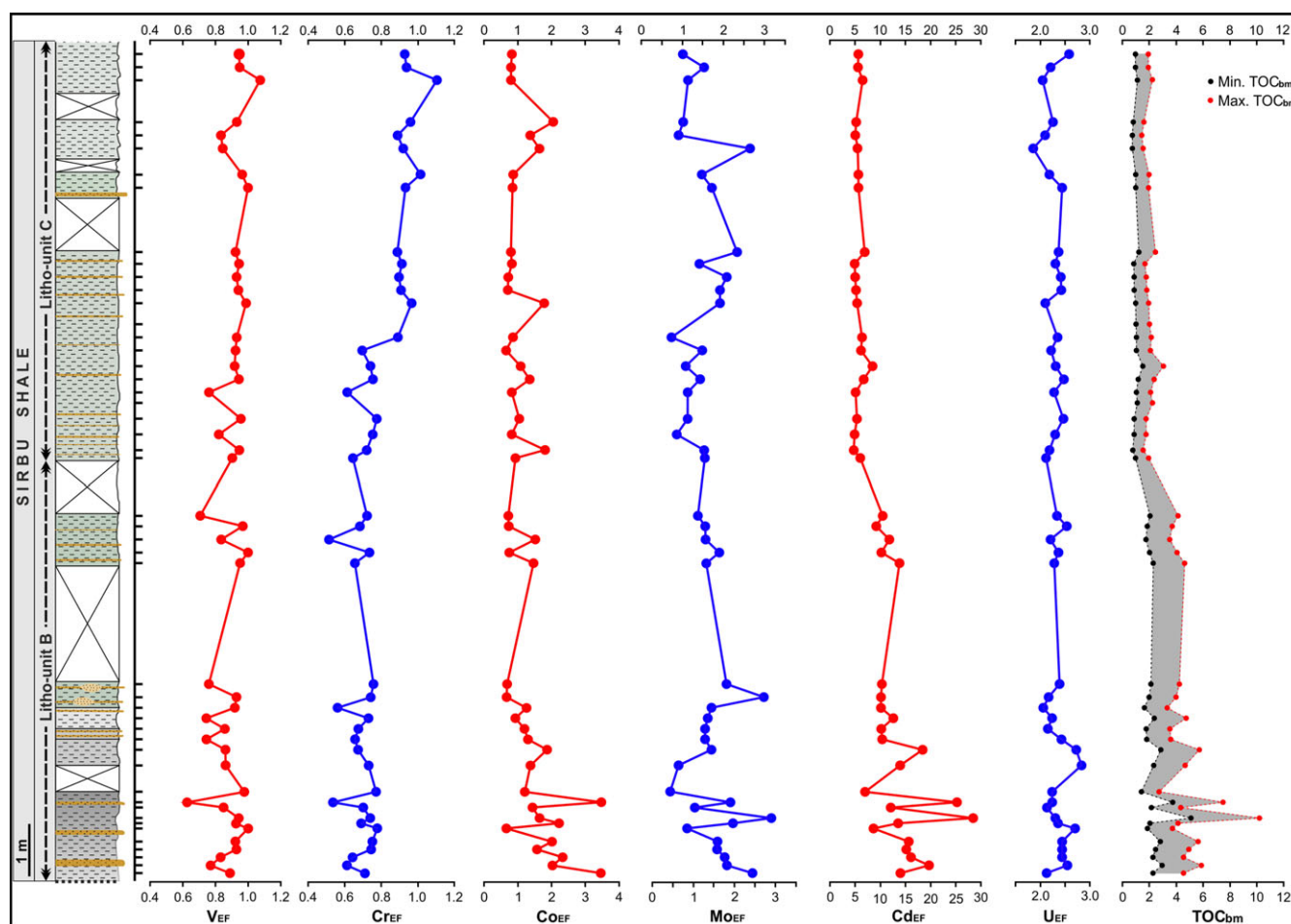


Fig. 3. (Colour online) Stratigraphic profile of V_{EF} , Cr_{EF} , Co_{EF} , Ni_{EF} , Mo_{EF} , Cd_{EF} , U_{EF} , TOC, $\delta^{13}C_{org}$, TOC_{bm} and TOC_{loss} for Sirbu Shale samples.

or poly-sulphide complexes (Gobeil *et al.* 1987; Plass *et al.* 2020; Chen *et al.* 2021). Given the limited post-depositional release of CdS from sediment (due to its lower solubility) in suboxic to anoxic settings (Bryan *et al.* 2021; Chen *et al.* 2021; Janssen *et al.* 2014, 2019), Cd seems more trustworthy among trace elements to be utilized as a proxy for palaeoproductivity and palaeoredox studies for non-euxinic sediments or rock deposits (Viehmann *et al.* 2019).

According to Morse and Luther III (1999), divalent trace metals such as Cd and Mn can form a sulphide mineral more quickly than iron and non-divalent trace metals (V, Cr, Ni, Co, Mo and U) because of their higher water exchange rates. Hence under the trace sulphide concentration, Cd and Mn are most likely to precipitate in considerable amounts when compared to V, Cr, Ni, Co, Mo and U. Additionally, compared to V, Cr, Ni, Co, Mo and U, the sulphide minerals of Cd and Mn are found more resistant to oxidative remobilization (Simpson *et al.* 1998). Thus, two possibilities could account for the large enrichment of Cd but no enrichment of V, Cr, Ni, Co and Mo in the Sirbu Shale: (1) the Sirbu Shale was deposited

in a suboxic environment with trace amounts of sulphide production that were enough to precipitate Cd, Mn and other divalent trace metals but no others; (2) The Sirbu Shale deposition took place under suboxic to an anoxic condition that precipitated a significant amount of divalent (Cd and Mn) as well as non-divalent trace metals (V, Cr, Ni, Co, Mo and U), but during the intermittent oxygenation of sediments, non-divalent sulphides redissolved rapidly into the overlying water column. In contrast, sulfides of divalent trace metals underwent little change. A significant positive correlation of Cd_{EF} with Mn/Al (Figure 5(b)) can be considered as evidence for little to no significant remobilization of Cd and Mn. But no correlation between Cd and Fe/Al (Figure 5(c)) suggests a significant remobilization of Fe during diagenetic history.

Additionally, over several million years, the maturation/thermal cracking of the organic matter in the sediment under high pressure and temperature conditions can result in the release of labile organic components in the form of liquids and gases, which can remobilise the trace elements as well (Ardakani *et al.*

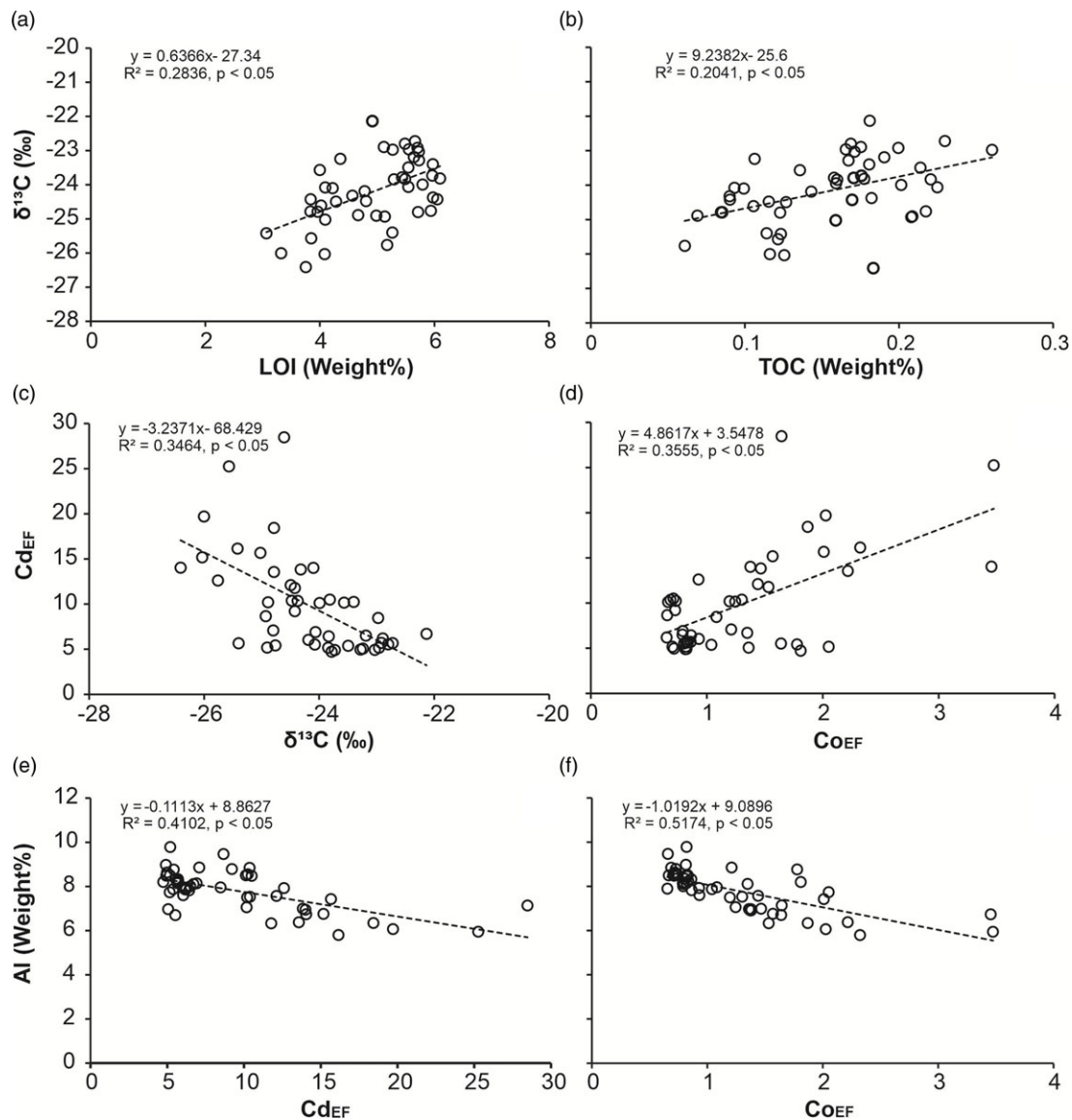


Fig. 4. The cross plots of (a) $\delta^{13}\text{C}$ versus TOC, (b) $\delta^{13}\text{C}$ versus LOI, (c) Cd_{EF} versus $\delta^{13}\text{C}$, (d) Cd_{EF} versus Co_{EF} , (e) Al versus Cd_{EF} and (f) Al versus Co_{EF} for Sirbu Shale samples.

2016; Wilde *et al.* 2004). A recent experimental study by Dickson *et al.* (2020), however, demonstrated that this process may lead to a loss of organic matter from the rocks and an increase in organically bound trace elements. A negative correlation of Cd_{EF} with TOC and LOI (Table 2b) in this study can be an indication of slight enrichment of Cd during TOC loss through cracking of sedimentary organic matter during rock maturation. Such changes in Cd concentration during the maturation process are minor in comparison to the bulk enrichment of Cd in the shale samples (Dickson *et al.* 2020) and can be disregarded.

Organic carbon isotope values during early diagenesis in a range of environments can change by ± 2.5 ‰ (Freudenthal *et al.* 2001; Lehmann *et al.* 2002). Typically, a decrease in $\delta^{13}\text{C}$ of organic matter has been reported during their degradation because ^{12}C -enriched organic compounds are relatively more stable/refractory than ^{13}C -enriched organic compounds (Freudenthal *et al.* 2001). Furthermore, studies have demonstrated that residual sedimentary organic matter of the oxic zone contains a lower

proportion of refractory organic matter compared to that of the anoxic zone, which suggests that the carbon isotope effect associated with organic matter remineralization in the anoxic zone would be higher than that occur in the oxic zone (Jochum *et al.* 1995; Partin *et al.* 2013; Lindsey *et al.* 2018). This shows that the significant positive correlation of TOC with $\delta^{13}\text{C}$ and LOI (Figures 4(a), (b)) observed in the Sirbu Shale samples can be a result of the isotopic effect associated with the remineralization of sedimentary organic matter.

5.2. Palaeoredox environment and trace metal enrichment

The RSTEs, which are water-soluble in oxidized form and water-insoluble in reduced form, i.e., Cr and V, show no enrichment. It can be explained by either depletion of these trace metals in source rocks, i.e., terrestrial felsic rocks (Morris, 1986; Paikaray *et al.* 2008; Absar *et al.* 2009; Banerjee & Banerjee, 2010) or their progressive loss in low salinity water (Morris, 1986; O'Connor *et al.* 2015). The

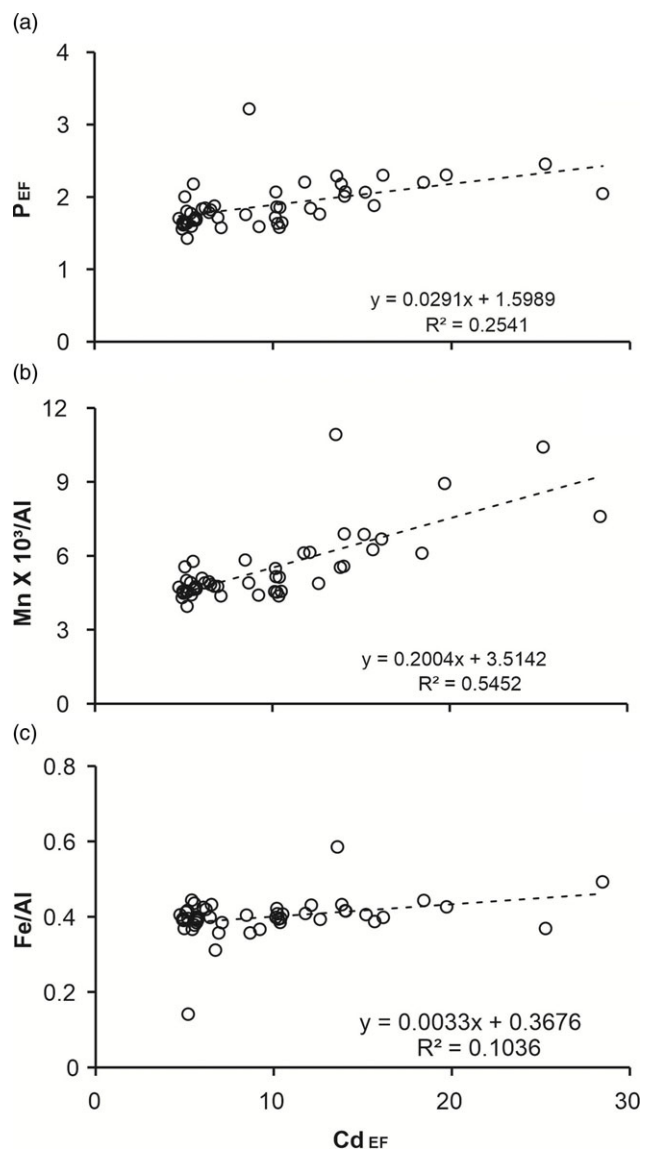


Fig. 5. The cross plots of (a) P_{EF} versus Cd_{EF} , (b) Mn/Al versus Cd_{EF} , and (c) Fe/Al versus Cd_{EF} for Sirbu Shale samples.

trace elements ratios such as Th/Co and Th/Cr , which are found significantly different for felsic and mafic rocks (Nagarajan *et al.* 2007), suggest a predominant felsic source for the Sirbu Shale (Table 3). The U_{EF} of the Sirbu Shale ranging, between 1.8 and 2.8, is consistent with the modern marine sediments deposited in suboxic conditions or nitrate reduction zone (Algeo & Li, 2020; Kessarkar *et al.* 2022). Small intermittent enrichment of Co could be associated with its co-precipitation along with Cd in the organic matter or with the trace of sulphides, which is evident from the significant positive correlation between Cd_{EF} and Co_{EF} (Figure 4(d)). Furthermore, Cd_{EF} and Co_{EF} show a significant negative correlation with detrital tracer element Al (Figure 4(e), (f)), which supports the notion that their large proportion in the sediments was associated with non-detrital deposition (Rosenthal *et al.* 1995; Janssen *et al.* 2014; Dickson *et al.* 2020). The adsorption of Cd and Co on the clay minerals, which tends to increase with a rise in Mn^{2+} concentration, could also have immobilized them in addition to organic matter and sulphides in a suboxic to the anoxic

environment (Groeningen *et al.* 2020). A statistically significant moderate positive correlation among Cd_{EF} , Co_{EF} and Mn (Figure 4 and Table 2b) supports the latter possibility.

The sourcing of Cd and Co, as well as Mn, was most likely from the upwelling region in the relatively deeper marine shelf region (Wagner *et al.* 2013; Sweere *et al.* 2016, 2020). The relatively high enrichment level of Cd but no significant enrichment of other trace elements in the Sirbu Shale closely matches with the modern marine surface sediments underlying the suboxic zone of Chile margins (Böning *et al.* 2005), which is one of the most prominent seasonal upwelling zones in the modern ocean. This suggests that the Sirbu Shale was deposited in a setting similar to that in which modern suboxic sediments of the Chilean margin are deposited. In light of this conclusion, the substantial enrichment of Cd in the shale, but the lack of considerable enrichment in other trace elements, can also be utilized as a palaeo-indicator of a suboxic marine environment driven by seasonal upwelling. However, testing this hypothesis will require more such data from black shale deposits and modern anoxic basins.

5.3. Palaeoproductivity

In marine/freshwater basins, during the transit from primary production (photosynthesis) to burial in sediments, organic matter undergoes rapid remineralization, which is mainly controlled by water column oxygen condition, type of organic matter exported (more refractory or more labile) and sedimentation rate (Burdige, 2007). The efficiency of this process is found variable on the spatial scale (Lutz *et al.* 2007) and over geological time (Raven & Falkowski, 1999). It has been found that under oxygenated marine water column conditions, less than 0.5% of organic matter from gross primary production reaches the sediments (Burdige, 2007), therefore not a true representative of primary productivity (Lopes *et al.* 2015). In the Sirbu Shale, TOC contents remain persistently below 0.26% (Table 2a) with an average value of 0.18%, suggesting that either primary productivity was originally low, or if primary productivity was high, the burial efficiency of photosynthetically derived organic matter was poor due to frequent ventilation of the water column and/or low sedimentation rate. Under these circumstances, Cd released from the remineralization of organic matter moves towards the oxic-anoxic boundary in the subsurface sediment due to a concentration gradient caused by Cd precipitation with sulphide traces in suboxic-anoxic zones. Therefore, Cd can provide a more accurate depiction of the primary production than TOC itself, preserved in ancient sedimentary records. The Cd_{EF} in this study shows a weak but statistically significant (Pearson coefficient = 0.000355) correlation (Figure 5(a) and Table 2b) with P_{EF} , demonstrating a small enrichment compared to UCC. Since P is an essential nutrient that controls the oceanic primary productivity and organic matter export to the sediment is one of the most important contributors to sedimentary P content in marine environment, the enrichment of P in marine sedimentary records is also used as a strong proxy for delineating palaeoproductivity (Ruttenberg and Berner, 1993; Schenau *et al.* 2005). However, a large fraction of P from sedimentary organic matter is often released back into the water column during early diagenesis remineralization (Ruttenberg and Berner, 1993; Sulu-Gambari *et al.* 2018). The phosphorus content in the Sirbu Shale is found comparative to the sediments of a seasonally hypoxic modern marine basin (Schenau *et al.* 2005). Thus, the enrichment of Cd and P and a significant correlation

Sirbu Shale palaeodepositional environment and palaeoproductivity

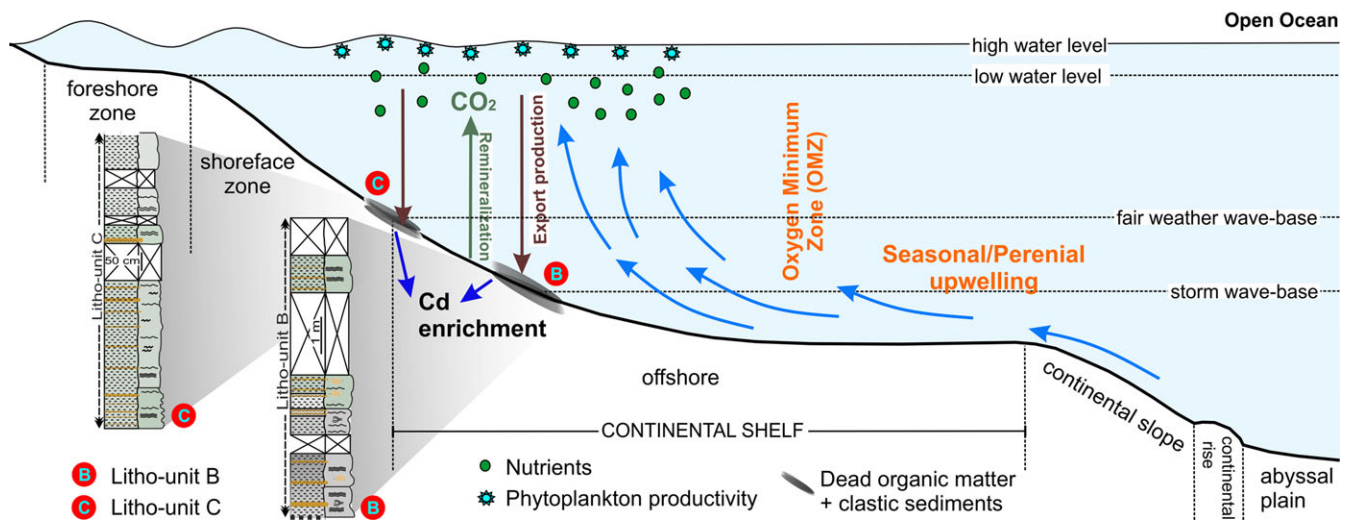


Fig. 6. (Colour online) Schematic diagram of Sirbu Shale palaeodepositional environment and palaeoproductivity. B in the figure denotes the palaeodepositional position of litho-units B and C denotes the palaeodepositional position of litho-unit C in the basin.

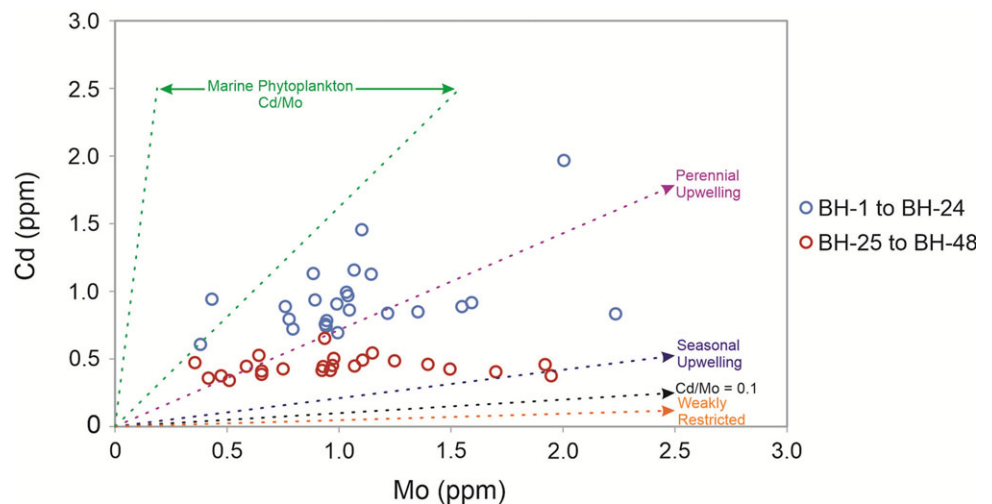


Fig. 7. (Colour online) Mo versus Cd plot for Sirbu Shale samples with regression lines forced through the origin, representing Cd/Mo ratios for marine phytoplankton, perennial upwelling, seasonal upwelling, and weakly restricted conditions. This figure is adapted from Sweere *et al.* (2016).

between the two in Sirbu Shale can be considered compelling evidence of high primary productivity in the concomitant depositional environment.

The average minimum and maximum TOC_{bm} (organic matter that made it to the sediment through the water column) calculated using Eq. 4, for the Sirbu Shale, are 1.65 and 3.31%, respectively. These average TOC_{bm} values closely overlap the TOC values (1.53 to 3.45%) reported from the modern marine sediments underlying the suboxic waters of Chile margin's oxygen minimum zone, which are subject to substantial seasonal upwelling and high primary productivity (Böning *et al.* 2005). TOC_{bm} shows an overall stratigraphic decrease in the studied section of the Sirbu Shale (Figure 3). This stratigraphic variation of TOC_{bm} indicates that the litho-unit B was deposited under relatively higher productivity and less ventilated conditions compared to the litho-unit C. The average TOC_{loss} (calculated by subtracting the bulk TOC value of sample from the TOC_{bm}) through remineralization during the deposition of the litho-unit B ranging from 94 to 97% was

noticeably higher than during the deposition of the litho-unit C, which has the average TOC_{loss} ranged from 82 to 91% (see Supplementary Table 3). These results indicate that the TOC_{loss} through diagenesis/remineralization during the higher primary productivity was relatively higher and vice-versa. As the sedimentological studies of Sirbu Shale suggest that litho-unit B was deposited in a relatively deeper sea-shelf environment (around storm wave-base) compared to litho-unit C (deposited near fair weather wave-base) (Figure 6; Singh & Chakraborty, 2022), the higher TOC_{loss} in litho-unit B seems to be a result of relatively slower sedimentation rate. According to studies of marine sediments, $\text{TOC}_{\text{loss}} > 80\%$ through remineralization in marine sediments is generally associated with the sediments underlying suboxic to oxic water column (Burdige, 2007). These shifts in the primary productivity might have been driven by changes in nutrient supply through terrestrial discharge and/or through an upwelling-productivity feedback loop over the continental shelf (Pedersen & Calvert, 1990; Wyrтки, 1962).

5.4 Upwelling and basin restriction

The Cd/Mo ratios in Sirbu Shale are greater than 0.36 (Figure 7), implying that the studied section was most likely deposited in an open marine shelf condition. Furthermore, Figure 7, adapted from Sweere *et al.* (2016), shows that Cd/Mo ratios of litho-unit B fall in the perennial upwelling zone, and Cd/Mo ratios of litho-unit C fall in the seasonal upwelling zone. Detailed comparison of the Sirbu Shale Cd/Mo data with the trace metal data from oxygen-depleted basins (Sweere *et al.* 2016 and reference therein) reveals more similarity with the sediment core records of the Arabian Sea (average Cd/Mo = 0.14) (Van der Weijden *et al.* 2006) and the Gulf of California (average Cd/Mo ratio = 0.21) (Brumsack, 1989), which are known for seasonal upwelling condition. Sedimentary Cd/Mo ratios in hydrographically restricted basins are generally found close to that in seawater composition (average Cd/Mo ~ 0.0057, Sarmiento *et al.* 2004) but an increase in the influence (frequency) of upwelling leads to a Cd/Mo ratio closer to the phytoplankton composition (average Cd/Mo ~ 7.9, Ho *et al.* 2003). Therefore, the accumulations of Cd-rich phytoplankton reaching the sediments in upwelling-induced high productivity settings are likely to contribute a strong Cd enrichment (Sweere *et al.* 2016, 2020).

Given the above interpretation, we must admit that basin morphology, redox structure (i.e., coverage of anoxic and euxinic sea floor) and terrestrial influx in the Precambrian basins might be substantially different from the modern anoxic basins. For example, studies have demonstrated that trace metal drawdown in the Proterozoic ocean was perhaps greater than today due to larger coverage of anoxic and euxinic sea seafloor, which would have varied over the geological time scale (Reinhard *et al.* 2013, 2016). Therefore, we are sceptical about to what extent such a trace metal ratio model based on modern anoxic basin studies can accurately interpret the Precambrian oceanic environment. It remains a question that must be debated and addressed in future studies.

6. Conclusion

In the post-NOE, Precambrian Ocean productivity varied from moderate to high depending upon the varying intensity of nutrient supply through upwelling in deeper marine shelf regions. However, TOC from the rock records does not reflect these variations in productivity because of high TOC_{loss} through remineralization in the water column as well as in the surface sediment during early diagenesis resulting in a very low TOC content in the sedimentary rock record, which on stratigraphic scale appears almost invariable. This study demonstrated that authigenic Cd enrichment in sedimentary rocks can be used with fair confidence to estimate total organic matter exported to the seafloor during deposition. However, more such studies are recommended to strengthen this finding. The following are the key findings of this study:

- This study demonstrated that the Sirbu Shale was deposited in a hydrographically restricted open marine shelf environment, which experienced strong upwelling and led to high primary productivity.
- The findings imply that the deposition of the Sirbu Shale occurred in the close vicinity of a major marine oxygen minimum zone.

- During the deposition of litho-unit B of Sirbu Shale, the average TOC exported to the sediments ranged from 2.3 to 4.6%, and 93 to 96% of it was lost through remineralization during diagenesis. Whereas during the deposition of litho-unit C of Sirbu Shale, average TOC exported to the sediments varied from 1 to 2%, and 81 to 91% of it was lost through remineralization during diagenesis.

Supplementary material. The supplementary material for this article can be found at <https://doi.org/10.1017/S0016756823000614>

Acknowledgement. We are thankful to the Director of BSIP for throughout support. Lab work was performed by Dr. Shailesh Agarwal, Archana Sonkar, Ishwar Rahi and Sandeep Kohri. The help of Yogesh Kumar in data visualization/artwork is very much appreciated. We are grateful to the two anonymous reviewers for their comments and suggestions, which were immensely helpful in improving the MS.

Funding Statement. This work was funded by BSIP under Project 1 (2021-2025). The BSIP contribution number for this MS is BSIP/RDCC/Publication no. 84/2020-21.

References

- Absar N, Raza M, Roy M, Naqvi S and Roy AK (2009) Composition and weathering conditions of Paleoproterozoic upper crust of Bundelkhand craton, Central India: records from geochemistry of clastic sediments of 1.9 Ga Gwalior Group. *Precambrian Research* **168**, 313–329. <https://doi.org/10.1016/j.precamres.2008.11.001>
- Agrawal S, Srivastava P, Sonam Meena NK, Rai SK, Bhushan R, Misra DK and Gupta AK (2015) Stable ($\delta^{13}\text{C}$ and $\delta^{15}\text{N}$) isotopes and magnetic susceptibility record of late Holocene climate change from a lake profile of the northeast Himalaya. *Journal of the Geological Society of India* **86**, 696–705. <https://doi.org/10.1007/s12594-015-0362-9>
- Algeo TJ and Li C (2020) Redox classification and calibration of redox thresholds in sedimentary systems. *Geochimica et Cosmochimica Acta* **287**, 8–26. <https://doi.org/10.1016/j.gca.2020.01.055>
- Anbar AD and Knoll AH (2002) Proterozoic ocean chemistry and evolution: a bioinorganic bridge? *Science* **297**, 1137–1142. <https://doi.org/10.1126/science.1069651>
- Ansari AH, Ahmad S, Govil P, Agrawal S and Mathews RP (2020) Mo-Ni and organic carbon isotope signatures of the mid-late Mesoproterozoic oxygenation. *Journal of Asian Earth Science* **191**, 104201. <https://doi.org/10.1016/j.jseas.2019.104201>
- Ansari AH, Pandey S K, Sharma M, Agrawal S and Kumar Y (2018) Carbon and oxygen isotope stratigraphy of the Ediacaran Bilara Group, Marwar Supergroup, India: evidence for high amplitude carbon isotopic negative excursions. *Precambrian Research* **308**, 75–91. <https://doi.org/10.1016/j.precamres.2018.02.002>
- Ansari AH, Singh VK, Sharma M and Kumar K (2022) High authigenic Co enrichment in the non-euxinic buff-grey and black shale of the Chandarpur Group, Chhattisgarh Supergroup: implication for the late Mesoproterozoic shallow marine redox condition. *Terra Nova* **34**(1), 72–82. <https://doi.org/10.1111/ter.12564>
- Ardakani OH, Chappaz A, Sanei H and Mayer B (2016) Effect of thermal maturity on remobilization of molybdenum in black shales. *Earth Planetary Science Letters* **449**, 311–320. <https://doi.org/10.1016/j.epsl.2016.06.004>
- Banerjee A and Banerjee D (2010) Modal analysis and geochemistry of two sandstones of the Bhandar Group (Late Neoproterozoic) in parts of the Central Indian Vindhyan basin and their bearing on the provenance and tectonics. *Journal of Earth System Science* **119**, 825. <https://doi.org/10.1007/s12040-010-0056-z>
- Bhattacharyya A (1993) *The Upper Vindhyan of Maihar-Field Guide*. Geological Society of India, Bangalore, India. 98 pp.

- Bhattacharyya A** (1996) *Foreword*. Geological Society of India Memoir, 36, ii–viii.
- Böning P, Cuypers S, Grunwald M, Schnetger B and Brumsack HJ** (2005) Geochemical characteristics of Chilean upwelling sediments at ~36°S. *Marine Geology* **220**(1–4), 1–21. <https://doi.org/10.1016/j.margeo.2005.07.005>
- Boyle EA, Sclater F and Edmond J** (1976) On the marine geochemistry of cadmium. *Nature* **263**, 42–44. <https://doi.org/10.1038/263042a0>
- Brumsack HJ** (1989) Geochemistry of recent TOC-rich sediments from the Gulf of California and the Black Sea. *Geologische Rundschau* **78**(3), 851–882. <https://doi.org/10.1007/BF01829327>
- Brumsack HJ** (2006) The trace metal content of recent organic carbon-rich sediments: implications for Cretaceous black shale formation. *Palaeogeography, Palaeoclimatology, Palaeoecology* **232**, 344–361. <https://doi.org/10.1016/j.palaeo.2005.05.011>
- Bryan AL, Dickson AJ, Dowdall F, Homoky WB, Porcelli D and Henderson GM** (2021) Controls on the cadmium isotope composition of modern marine sediments. *Earth and Planetary Science Letters* **565**, 116946. <https://doi.org/10.1016/j.epsl.2021.116946>
- Burdige DJ** (2007) Preservation of organic matter in marine sediments: controls, mechanisms, and an imbalance in sediment organic carbon budgets? *Chemical Reviews* **107**, 467–485. <https://doi.org/10.1021/cr050347q>
- Canfield DE, Poulton SW and Narbonne GM** (2007) Late-Neoproterozoic deep-ocean oxygenation and the rise of animal life. *Science* **315**, 92–95. <https://doi.org/10.1126/science.1135013>
- Cawood PA, Zhao G, Yao J, Wang W, Xu Y and Wang Y** (2018) Reconstructing South China in Phanerozoic and Precambrian supercontinents. *Earth Science Reviews* **186**, 173–194. <https://doi.org/10.1016/j.earscirev.2017.06.001>
- Chen L, Little SH, Kreissig K, Severmann S and McManus J** (2021) Isotopically light Cd in sediments underlying oxygen deficient zones. *Frontiers in Earth Science* **9**, 623720. <https://doi.org/10.3389/feart.2021.623720>
- Crawford AR and Compston W** (1969) The age of the Vindhyan system of peninsular India. *The Quarterly Journal of the Geological Society of London* **125**, 351–371. <https://doi.org/10.1144/gsjgs.125.1.0351>
- Cullen JT** (2006) On the nonlinear relationship between dissolved cadmium and phosphate in the modern global ocean: could chronic iron limitation of phytoplankton growth cause the kink? *Limnology and Oceanography* **51**, 1369–1380. <https://doi.org/10.4319/lo.2006.51.3.1369>
- Cullers RL** (1994) The controls on the major and trace element variation of shales, siltstones, and sandstones of Pennsylvanian-Permian age from uplifted continental blocks in Colorado to platform sediment in Kansas, USA. *Geochimica et Cosmochimica Acta* **58**(22), 4955–4972. [https://doi.org/10.1016/0016-7037\(94\)90224-0](https://doi.org/10.1016/0016-7037(94)90224-0)
- Cullers RL** (2000) The geochemistry of shales, siltstones and sandstones of Pennsylvanian-Permian age, Colorado, USA: implications for provenance and metamorphic studies. *Lithos* **51**(3), 181–203. [https://doi.org/10.1016/S0024-4937\(99\)00063-8](https://doi.org/10.1016/S0024-4937(99)00063-8)
- De C** (2003) Possible organisms similar to Ediacaran forms from the Bhandar Group, Vindhyan Supergroup, late Neoproterozoic of India. *Journal of Asian Earth Science* **21**(4), 387–395. [https://doi.org/10.1016/S1367-9120\(02\)00036-6](https://doi.org/10.1016/S1367-9120(02)00036-6)
- De C** (2006) Ediacara fossil assemblage in the upper Vindhyan of central India and its significance. *Journal of Asian Earth Science* **27**(5), 660–683. <https://doi.org/10.1016/j.jseaes.2005.06.006>
- De C** (2009) The Vindhyan Ediacaran fossil and trace fossil assemblages; their insights into early metazoan palaeobiology, palaeobiogeography and Vindhyan biostratigraphy. *Indian Journal of Geosciences* **63**(1), 11–40.
- Deb SP** (2004) Lithostratigraphy of the Neoproterozoic Chattisgarh Sequence, its bearing on the tectonics and palaeogeography. *Gondwana Research* **7**, 323–337. [https://doi.org/10.1016/S1342-937X\(05\)70787-5](https://doi.org/10.1016/S1342-937X(05)70787-5)
- Dickson AJ, Idiz E, Porcelli D and van den Boorn SH** (2020) The influence of thermal maturity on the stable isotope compositions and concentrations of molybdenum, zinc and cadmium in organic-rich marine mudrocks. *Geochimica et Cosmochimica Acta* **287**, 205–220. <https://doi.org/10.1016/j.gca.2019.11.001>
- Erwin DH, Laflamme M, Tweedt SM, Sperling EA, Pisani D and Peterson KJ** (2011) The Cambrian conundrum: early divergence and later ecological success in the early history of animals. *Science* **334**, 1091–1097. <https://doi.org/10.1126/science.1206375>
- Freudenthal T, Wagner T, Wenzhöfer F., Zabel M and Wefer G** (2001) Early diagenesis of organic matter from sediments of the eastern subtropical Atlantic: evidence from stable nitrogen and carbon isotopes. *Geochimica et Cosmochimica Acta* **65**, 1795–1808. [https://doi.org/10.1016/S0016-7037\(01\)00554-3](https://doi.org/10.1016/S0016-7037(01)00554-3)
- Friedman G and Chakraborty C** (1997) Stable isotopes in marine carbonates: their implications for the paleoenvironment with special reference to the Proterozoic Vindhyan carbonates (Central India). *Journal of Geological Society of India* **50**, 131–159.
- Friedman GM, Chakraborty C and Kolkas MM** (1996) $\delta^{13}\text{C}$ excursion in the End-Proterozoic strata of the Vindhyan basin (central India): its chronostratigraphic significance. *Carbonate and Evaporite* **11**, 206–212. <https://doi.org/10.1007/BF03175638>
- Gendron A, Silverberg N, Sundby B and Lebel J** (1986) Early diagenesis of cadmium and cobalt in sediments of the Laurentian Trough. *Geochimica et Cosmochimica Acta* **50**, 741–747. [https://doi.org/10.1016/0016-7037\(86\)90350-9](https://doi.org/10.1016/0016-7037(86)90350-9)
- Georgiev SV, Horner TJ, Stein HJ, Hannah JL, Bingen B and Rehkämper M** (2015) Cadmium-isotopic evidence for increasing primary productivity during the Late Permian anoxic event. *Earth and Planetary Science Letters* **410**, 84–96. <https://doi.org/10.1016/j.epsl.2014.11.010>
- Gladkochub DP, Donskaya TV, Stanevich AM, Pisarevsky SA, Zhang S, Motova ZL, Mazukabzov AM and Li H** (2019) U-Pb detrital zircon geochronology and provenance of Neoproterozoic sedimentary rocks in southern Siberia: new insights into breakup of Rodinia and opening of Paleo-Asian Ocean. *Gondwana Research* **65**, 1–16. <https://doi.org/10.1016/j.gr.2018.07.007>
- Gobeil C, Silverberg N, Sundby B and Cossa D** (1987) Cadmium diagenesis in Laurentian Trough sediments. *Geochimica et Cosmochimica Acta* **51**(3), 589–596. [https://doi.org/10.1016/0016-7037\(87\)90071-8](https://doi.org/10.1016/0016-7037(87)90071-8)
- Gopalan K, Kumar A, Kumar S and Vijaygopal B** (2013) Depositional history of the Upper Vindhyan succession, central India: time constraints from Pb-Pb isochron ages of its carbonate components. *Precambrian Research* **233**, 108–117.
- Groeningen NV, Glück B, Christl I and Kretzschmar R** (2020) Surface precipitation of Mn 2+ on clay minerals enhances Cd 2+ sorption under anoxic conditions. *Environmental Science: Processes & Impacts* **22**(8), 1654–1665. <https://doi.org/10.1039/D0EM00155D>
- Hendry KR, Rickaby RE, de Hoog JC, Weston K and Rehkämper M** (2008) Cadmium and phosphate in coastal Antarctic seawater: implications for Southern Ocean nutrient cycling. *Marine Chemistry* **112**, 149–157. <https://doi.org/10.1016/j.marchem.2008.09.004>
- Ho TY, Quigg A, Finkel ZV, Milligan AJ, Wyman K, Falkowski PG and Morel FM** (2003) The elemental composition of some marine phytoplankton. *Journal of Phycology* **39**(6), 1145–1159. <https://doi.org/10.1111/j.0022-3646.2003.03-090.x>
- Hohl S, Galer S, Gamper A and Becker H** (2017) Cadmium isotope variations in Neoproterozoic carbonates—A tracer of biologic production? *Geochemical Perspectives Letters* **3**, 32–44. doi: 10.7185/geochemlet.1704
- Hohl SV, Jiang SY, Viehmann S, Wei W, Liu Q, Wei HZ and Galer SJ** (2020) Trace metal and Cd isotope systematics of the basal Datangpo Formation, Yangtze Platform (South China) indicate restrained (bio) geochemical metal cycling in Cryogenian seawater. *Geosciences* **10**(1), 36. <https://doi.org/10.3390/geosciences10010036>
- Hohl SV, Jiang SY, Wei HZ, Pi DH, Liu Q, Viehmann S and Galer SJ** (2019) Cd isotopes trace periodic (bio) geochemical metal cycling at the verge of the Cambrian animal evolution. *Geochimica et Cosmochimica Acta* **263**, 195–214. <https://doi.org/10.1016/j.gca.2019.07.036>
- Janssen DJ, Abouchami W, Galer SJG, Purdon KB and Cullen JT** (2019) Particulate cadmium stable isotopes in the subarctic northeast Pacific reveal dynamic Cd cycling and a new isotopically light Cd sink. *Earth and Planetary Science Letters* **515**, 67–78. <https://doi.org/10.1016/j.epsl.2019.03.006>

- Janssen DJ, Conway TM, John SG, Christian JR, Kramer DI, Pedersen TF and Cullen JT (2014) Undocumented water column sink for cadmium in the open ocean oxygen-deficient zones. *Proceedings of the National Academy of Sciences USA* **111**(19), 6888–6893. <https://doi.org/10.1073/pnas.1402388111>
- Jiang YY, Kong DX, Qin T, Li X, Caetano-Anolles G and Zhang HY (2012) The impact of oxygen on metabolic evolution: a chemoinformatic investigation. *PLOS Computational Biology* **8**, e1002426. <https://doi.org/10.1371/journal.pcbi.1002426>
- Jin C, Li C, Algeo TJ, Planavsky NJ, Cui H, Yang X, Zhao Y, Zhang X and Xie S (2016) A highly redox-heterogeneous ocean in South China during the early Cambrian (~529–514 Ma): implications for biota-environment co-evolution. *Earth and Planetary Science Letters* **441**, 38–51. <https://doi.org/10.1016/j.epsl.2016.02.019>
- Jochum J, Friedrich G, Leythaeuser D, Littke R and Ropertz B (1995) Hydrocarbon-bearing fluid inclusions in calcite-filled horizontal fractures from mature Posidonia Shale (Hils Syncline, NW Germany). *Ore Geology Reviews* **9**, 363–370. [https://doi.org/10.1016/0169-1368\(94\)00019-K](https://doi.org/10.1016/0169-1368(94)00019-K)
- John SG, Kunzmann M, Townsend EJ and Rosenberg AD (2017) Zinc and cadmium stable isotopes in the geological record: a case study from the post-snowball Earth Nuccaleena cap dolostone. *Palaeogeography, Palaeoclimatology, Palaeoecology* **466**, 202–208. <https://doi.org/10.1016/j.palaeo.2016.11.003>
- Jokhan Ram, Shukla SN, Pramanik AG, Verma BK, Chandra G and Murthy MSN (1996) Recent investigation in Vindhyan Basin: implications for the Basin tectonics. *Geological Society of India Memoir* **36**, 267–286.
- Kessarkar PM, Fernandes LL, Parthiban G, Kurian S, Shenoy DM, Pattan JN, Rao VP, Naqvi SWA and Verma S (2022) Geochemistry of sediments in contact with oxygen minimum zone of the eastern Arabian Sea: proxy for palaeo-studies. *Journal of Earth System Science* **131**(2), 91. <https://doi.org/10.1007/s12040-022-01823-2>
- Knoll AH (2011) The multiple origins of complex multicellularity. *Annual Review of Earth and Planetary Sciences* **39**, 217–239. <https://doi.org/10.1146/annurev.earth.031208.100209>
- Krishnan MS (1968) *Geology of India and Burma*. Madras, India: Higginbothams (P) Ltd. 211 pp.
- Krishnan MS and Swaminath J (1959) The Great Vindhyan Basin of northern India. *Journal of the Geological Society of India* **1**, 10–36.
- Kumar B, Das Sharma S, Sreenivas B, Dayal AM, Rao MN, Dubey N and Chawla BR (2002) Carbon, oxygen and strontium isotope geochemistry of Proterozoic carbonate rocks of the Vindhyan Basin, central India. *Precambrian Research* **113**(1–2), 43–63. [https://doi.org/10.1016/S0301-9268\(01\)00199-1](https://doi.org/10.1016/S0301-9268(01)00199-1)
- Kumari V, Tandon SK, Tomson JK and Ghatak A (2023) Detrital zircon U-Pb ages of Proterozoic and Cretaceous sandstones of Narmada region in Central India: Implications for provenance and the closure age of the Vindhyan Basin. *EarthArXiv.org*. <https://doi.org/10.31223/X5D94R>
- Kumar S (1976a) Stromatolites from the Vindhyan rocks of Son Valley- Maihar area, districts Mirzapur (U. P.) and Satna (M. P.). *Journal of the Palaeontological Society of India* **18**, 13–21.
- Kumar S (1976b) Significance of stromatolites in the correlation of Semri Series (Lower Vindhyan) of Son Valley and Chitrakut area, M. P. *Journal of the Palaeontological Society of India* **19**, 24–27.
- Kumar S (1999) Siliceous sponge spicule-like forms from the Neoproterozoic Bhandar Limestone, Maihar area, Madhya Pradesh. *Journal of the Palaeontological Society of India* **44**, 141–148.
- Kumar S and Pandey SK (2008) *Arumberia* and associated fossils from the Neoproterozoic Maihar Sandstone, Vindhyan Supergroup, Central India. *Journal of the Palaeontological Society of India* **53**, 83–97.
- Kumar S, Schidlowski M and Joachimski MM (2005) Carbon isotope stratigraphy of the Palaeo-Neoproterozoic Vindhyan Supergroup, central India; implications for basin evolution and intrabasinal correlation. *Journal of the Palaeontological Society of India* **50**(1), 65–81.
- Kumar S and Sharma M (2012) *Vindhyan Basin, Son Valley area, Central India, Field Guide-4*. The Palaeontological Society of India, Lucknow, India. 145 pp.
- Kumar S and Srivastava P (1997) A note on the carbonaceous megafossils from the Neoproterozoic Bhandar Group, Maihar area, Madhya Pradesh. *Journal of the Palaeontological Society of India* **42**, 141–146.
- Kumar S and Srivastava P (2003) Carbonaceous megafossils from the Neoproterozoic Bhandar Group, Central India. *Journal of the Palaeontological Society of India* **48**, 139–154.
- Lan Z, Zhang S, Li XH, Pandey SK, Sharma M, Shukla Y, Ahmad S, Sarkar S and Zhai M (2020) Towards resolving the ‘jigsaw puzzle’ and age-fossil inconsistency within East Gondwana. *Precambrian Research* **345**, 105775. <https://doi.org/10.1016/j.precamres.2020.105775>
- Lane TW, Saito MA, George GN, Pickering IJ, Prince RC and Morel FM (2005) A cadmium enzyme from a marine diatom. *Nature* **435**, 42. <https://doi.org/10.1038/435042a>
- Lehmann MF, Bernasconi SM, Barbieri A and McKenzie JA (2002) Preservation of organic matter and alteration of its carbon and nitrogen isotope composition during simulated and in situ early sedimentary diagenesis. *Geochimica et Cosmochimica Acta* **66**, 3573–3584. [https://doi.org/10.1016/S0016-7037\(02\)00968-7](https://doi.org/10.1016/S0016-7037(02)00968-7)
- Lenton TM, Boyle RA, Poulton SW, Shields-Zhou GA and Butterfield NJ (2014) Co-evolution of eukaryotes and ocean oxygenation in the Neoproterozoic era. *Nature Geoscience* **7**, 257–265. <https://doi.org/10.1038/ngeo2108>
- Li C, Planavsky NJ, Shi W, Zhang Z, Zhou C, Cheng M, Tarhan LG, Luo G and Xie S (2015) Ediacaran marine redox heterogeneity and early animal ecosystems. *Scientific Reports* **5**, 17097. <https://doi.org/10.1038/srep17097>
- Lindsey DR, Rimmer SM and Anderson KB (2018) Are redox-sensitive geochemical proxies valid in mature shales? Unconventional Resources Technology Conference (URTEC), URTEC-2901011-MS. Houston, Texas, 23–25 July 2018. September 2018, 2854–2860 pp. <https://doi.org/10.15530/URTEC-2018-2901011>
- Lopes C, Kucera M and Mix AC (2015) Climate change decouples oceanic primary and export productivity and organic carbon burial. *Proceedings of the National Academy of Sciences USA* **112**, 332–335. <https://doi.org/10.1073/pnas.1410480111>
- Löschner BM, De Jong JT and De Baar HJ (1998) The distribution and preferential biological uptake of cadmium at 6° W in the Southern Ocean. *Marine Chemistry* **62**, 259–286. [https://doi.org/10.1016/S0304-4203\(98\)00045-0](https://doi.org/10.1016/S0304-4203(98)00045-0)
- Lutz MJ, Caldeira K, Dunbar RB and Behrenfeld MJ (2007) Seasonal rhythms of net primary production and particulate organic carbon flux to depth describe the efficiency of biological pump in the global ocean. *Journal of Geophysical Research: Oceans* **112**, C10011. <https://doi.org/10.1029/2006JC003706>
- Mahon RC, Dehler CM, Link PK, Karlstrom KE and Gehrels GE (2014) Geochronologic and stratigraphic constraints on the Mesoproterozoic and Neoproterozoic Pahrump Group, Death Valley, California: a record of the assembly, stability, and breakup of Rodinia. *GSA Bulletin* **126**, 652–664. <https://doi.org/10.1130/B30956.1>
- Malone SJ, Meert JG, Banerjee DM, Pandit MK, Tamrat J, Kamenov GD, Prashan VR and Sohl LI (2008) Paleomagnetism and detrital zircon geochemistry of the Upper Vindhyan sequence of Son Valley and Rajasthan: a ca. 1000 Ma closure age for the Purana Basin. *Precambrian Research* **164**, 137–159. <https://doi.org/10.1016/j.precamres.2008.04.004>
- Mathur S (1987) Geochronology and biostratigraphy of the Vindhyan Supergroup. *Visesa Prakasana-Bharatiya Bhuvaijñanika Sarveksana* **11**, 23–44.
- McCorkle DC and Klinkhammer GP (1991) Porewater cadmium geochemistry and the porewater cadmium: $\delta^{13}\text{C}$ relationship. *Geochimica et Cosmochimica Acta* **55**, 161–168. [https://doi.org/10.1016/0016-7037\(91\)90408-W](https://doi.org/10.1016/0016-7037(91)90408-W)
- McKenzie NR, Hughes NC, Myrow PM, Xiao S and Sharma M (2011) Correlation of Precambrian-Cambrian sedimentary successions across northern India and the utility of isotopic signatures of Himalayan lithotectonic zones. *Earth and Planetary Science Letters* **312**, 471–483. <https://doi.org/10.1016/j.epsl.2011.10.027>
- Meert JG, Pandit MK, Kwafo S and Singha A (2023) Stinging News: ‘Dickinsonia’ discovered in the Upper Vindhyan of India Not Worth the Buzz. *Gondwana Research* **117**, 1–7. <https://doi.org/10.1016/j.gr.2023.01.003>
- Meyer KM, Ridgwell A and Payne JL (2016) The influence of the biological pump on ocean chemistry: implications for long-term trends in marine redox chemistry, the global carbon cycle, and marine animal ecosystems. *Geobiology* **14**(3), 207–219. <https://doi.org/10.1111/gbi.12176>

- Misra Y and Kumar S (2005) Coniform stromatolites and the Vindhyan Supergroup, Central India: implication for basinal correlation and age. *Journal of the Palaeontological Society of India* **50**(2), 153–167.
- Mondal MEA, Goswami JN, Deomurari MP and Sharma KK (2002) Ion microprobe $^{207}\text{Pb}/^{206}\text{Pb}$ ages of zircons from the Bundelkhand massif, northern India: implications for crustal evolution of the Bundelkhand–Aravalli protocontinent. *Precambrian Research* **117**, 85–100. [https://doi.org/10.1016/S0301-9268\(02\)00078-5](https://doi.org/10.1016/S0301-9268(02)00078-5)
- Morel FM and Malcolm EG (2005) The biogeochemistry of cadmium. In *Metal Ions in Biological Systems* (eds A Sigel, H Sigel & RKO Sigel), pp. 195–219. Boca Raton: CRC Press. <https://doi.org/10.1201/9780824751999.ch8>
- Morris A (1986) Removal of trace metals in the very low salinity region of the Tamar Estuary, England. *Science of the Total Environment* **49**, 297–304. [https://doi.org/10.1016/0048-9697\(86\)90245-7](https://doi.org/10.1016/0048-9697(86)90245-7)
- Morse JW and Luther III GW (1999) Chemical influences on trace metal-sulfide interactions in anoxic sediments. *Geochimica et Cosmochimica Acta* **63**(19–20), 3373–3378. [https://doi.org/10.1016/S0016-7037\(99\)00258-6](https://doi.org/10.1016/S0016-7037(99)00258-6)
- Nagarajan R, Madhavaraju J, Nagendra R, Armstrong-Altrin JS and Moutte J (2007) Geochemistry of Neoproterozoic shales of the Rabanpalli Formation, Bhima Basin, Northern Karnataka, southern India: implications for provenance and paleoredox conditions. *Revista mexicana de ciencias geológicas* **24**(2), 150–160.
- O'Connor AE, Luek JL, McIntosh H and Beck AJ (2015) Geochemistry of redox-sensitive trace elements in a shallow subterranean estuary. *Marine Chemistry* **172**, 70–81. <https://doi.org/10.1016/j.marchem.2015.03.001>
- Paikaray S, Banerjee S and Mukherji S (2008) Geochemistry of shales from the Paleoproterozoic to Neoproterozoic Vindhyan Supergroup: implications on provenance, tectonics and paleoweathering. *Journal of Asian Earth Sciences* **32**, 34–48. <https://doi.org/10.1016/j.jseaes.2007.10.002>
- Pandey SK (2012) *Biozonation and Correlation of the Neoproterozoic Bhandar Group, India*. Germany: Lap Lambert Academic Publishing. 165 pp.
- Pandey SK, Ahmad S and Sharma M (2023a) *Dickinsonia tenuis* reported by Retallack et al. 2021 is not a fossil, instead an impression of an extant 'fallen beehive'. *Journal of the Geological Society of India* **99**, 1–6.
- Pandey SK and Kumar S (2013) Organic walled microbiota from the silicified Algal clasts, Bhandar Limestone, Satna Area, Madhya Pradesh. *Journal of the Geological Society of India* **82**, 499–508. <https://doi.org/10.1007/s12594-013-0181-9>
- Pandey SK, Singh D, Sharma M, Ahmad S, Bhan U (2023b) A new palaeobiological assemblage from the Son Valley Bhandar Group and its implications on the age of the upper Vindhyan of India. *Palaeoworld* (In Press). <https://doi.org/10.1016/j.palwor.2023.06.001>
- Partin CA, Bekker A, Planavsky NJ, Scott CT, Gill BC, Li C, Podkovyrov V, Maslov A, Konhauser KO, Lalonde SV, Love GD, Poulton SW and Lyons TW (2013) Large-scale fluctuations in Precambrian atmospheric and oceanic oxygen levels from the record of U in shales. *Earth and Planetary Science Letters* **369**, 284–293. <https://doi.org/10.1016/j.epsl.2013.03.031>
- Pedersen T and Calvert S (1990) Anoxia vs. productivity: what controls the formation of organic-carbon-rich sediments and sedimentary rocks? *AAPG Bulletin* **74**, 454–466. <https://doi.org/10.1306/0C9B232B-1710-11D7-8645000102C1865D>
- Plass A, Schlosser C, Sommer S, Dale AW, Achterberg EP and Scholz F (2020) The control of hydrogen sulfide on benthic iron and cadmium fluxes in the oxygen minimum zone off Peru. *Biogeosciences* **17**(13), 3685–3704.
- Prasad B (2007) *Obruchevella* and other terminal Proterozoic (Vendian) organic-walled microfossils from the Bhandar Group (Vindhyan Supergroup), Madhya Pradesh. *Journal of the Geological Society of India* **69**(2), 295–310.
- Prasad B, Uniyal SN and Asher R (2005) Organic-walled microfossils from the Proterozoic Vindhyan Supergroup of Son Valley, Madhya Pradesh, India. *Palaeobotanist* **54**(1–3), 13–60. <https://doi.org/10.54991/jop.2005.68>
- Preiss W and Forbes B (1981) Stratigraphy, correlation and sedimentary history of Adelaidean (Late Proterozoic) basins in Australia. *Precambrian Research* **15**, 255–304. [https://doi.org/10.1016/0301-9268\(81\)90054-1](https://doi.org/10.1016/0301-9268(81)90054-1)
- Price N and Morel F (1990) Cadmium and cobalt substitution for zinc in a marine diatom. *Nature* **344**, 658–660. <https://doi.org/10.1038/344658a0>
- Rai V, Shukla M and Gautam R (1997) Discovery of carbonaceous megafossils (*Chuarina-Tawuia* assemblage) from the Neoproterozoic Vindhyan succession (Rewa Group), Allahabad-Rewa area, India. *Current Science* **73**, 783–788.
- Rathore S, Vijan A, Krishna B, Prabhu B and Mishra K (1999) Dating of glauconite from Sirbu Shale of Vindhyan Supergroup, India. Proceedings of the 3rd International Petroleum Conference on Exploration, Petrotech, Delhi, India, 191–196 pp.
- Raven JA and Falkowski PG (1999) Oceanic sinks for atmospheric CO₂. *Plant, Cell & Environment* **22**, 741–755. <https://doi.org/10.1046/j.1365-3040.1999.00419.x>
- Ray JS, Martin MW, Veizer J and Bowring SA (2002) U–Pb zircon dating and Sr isotope systematics of the Vindhyan Supergroup, India. *Geology* **30**, 131–134. [https://doi.org/10.1130/0091-7613\(2002\)030%3C0131:UPZDAS%3E2.0.CO;2](https://doi.org/10.1130/0091-7613(2002)030%3C0131:UPZDAS%3E2.0.CO;2)
- Ray JS, Veizer J and Davis WJ (2003) C, O, Sr and Pb isotope systematics of carbonate sequences of the Vindhyan Supergroup, India; age, diagenesis, correlations and implications for global events. *Precambrian Research* **121**(1–2), 103–140. [https://doi.org/10.1016/S0301-9268\(02\)00223-1](https://doi.org/10.1016/S0301-9268(02)00223-1)
- Reinhard CT, Planavsky NJ, Gill BC, Ozaki K, Robbins LJ, Lyons TW, Fischer WW, Wang C, Cole DB and Konhauser KO (2017) Evolution of the global phosphorus cycle. *Nature* **541**, 386–389. <https://doi.org/10.1038/nature20772>
- Reinhard CT, Planavsky NJ, Olson SL, Lyons TW and Erwin DH (2016) Earth's oxygen cycle and the evolution of animal life. *Proceedings of the National Academy of Sciences of the United States of America* **113**(32), 8933–8938. <https://doi.org/10.1073/pnas.1521544113>
- Reinhard CT, Planavsky NJ, Robbins LJ, Partin CA, Gill BC, Lalonde SV, Bekker A, Konhauser KO and Lyons TW (2013) Proterozoic ocean redox and biogeochemical stasis. *Proceedings of the National Academy of Sciences of the United States of America* **110**(14), 5357–5362. <https://doi.org/10.1073/pnas.1208622110>
- Retallack GJ, Matthews NA, Master S, Khangar RG and Khan M (2021) *Dickinsonia* discovered in India and late Ediacaran biogeography. *Gondwana Research* **90**, 165–170. <https://doi.org/10.1016/j.gr.2020.11.008>
- Rogov V I, Karlova GA, Marusin VV, Kochnev BB, Nagovitsin KE and Grazhdankin DV (2015) Duration of the first biozone in the Siberian hypozostratotype of the Vendian. *Russian Geology and Geophysics* **56**, 573–583. <https://doi.org/10.1016/j.rgg.2015.03.016>
- Rooney AD, Austermann J, Smith EF, Yang L, Selby D, Dehler CM, Schmitz MD, Karlstrom KE and Macdonald FA (2018) Coupled Re–Os and U–Pb geochronology of the Tonian Chuar Group, Grand Canyon. *Geological Society of America Bulletin* **130**(7/8), 1085–1098. <https://doi.org/10.1130/B31768.1>
- Rosenthal Y, Lam P, Boyle EA and Thomson J (1995) Authigenic cadmium enrichments in suboxic sediments: precipitation and postdepositional mobility. *Earth and Planetary Science Letters* **132**, 99–111. [https://doi.org/10.1016/0012-821X\(95\)00056-1](https://doi.org/10.1016/0012-821X(95)00056-1)
- Rudnick RL & Gao S (2003) Composition of the continental crust. In *The Crust* (ed RL Rudnick), vol. 3 *Treatise on Geochemistry* (eds HD Holland & KK Turekian), pp. 1–64. Oxford: Elsevier. <https://doi.org/10.1016/B0-08-043751-6/03016-4>
- Ruttenberg KC and Berner RA (1993) Authigenic apatite formation and burial in sediments from non-upwelling, continental margin environments. *Geochimica et Cosmochimica Acta* **57**(5), 991–1007. [https://doi.org/10.1016/0016-7037\(93\)90035-U](https://doi.org/10.1016/0016-7037(93)90035-U)
- Sahoo SK, Planavsky NJ, Jiang G, Kendall B, Owens J, Wang X, Shi X, Anbar A and Lyons T (2016) Oceanic oxygenation events in the anoxic Ediacaran ocean. *Geobiology* **14**, 457–468. <https://doi.org/10.1111/gbi.12182>
- Sahoo SK, Planavsky NJ, Kendall B, Wang X, Shi X, Scott C, Anbar AD, Lyons TW and Jiang G (2012) Ocean oxygenation in the wake of the Marinoan glaciation. *Nature* **489**, 546–549. <https://doi.org/10.1038/nature11445>
- Sarkar S, Chakraborty S, Banerjee S and Bose P (2002) Facies sequence and cryptic imprint of sag tectonics in late Proterozoic Sirbu Shale, central India. In *Precambrian Sedimentary Environments: A Modern Approach to Ancient Depositional Systems Volume 33* (eds W Alterman & PL Corcoran), pp. 339–350. International Association of Sedimentologists, Blackwell Science Ltd, U.K. <https://doi.org/10.1002/9781444304312.ch17>

- Sarmiento JL, Gruber N, Brzezinski MA and Dunne JP (2004) High-latitude controls of thermocline nutrients and low latitude biological productivity. *Nature* **427**(6969), 56–60. <https://doi.org/10.1038/nature02127>
- Sastry MA and Moitra A (1984) Vindhyan stratigraphy—A review. *Geological Survey of India Memoir* **116**, 109–148.
- Schenu S, Reichart GJ and De Lange GJ (2005) Phosphorus burial as a function of paleoproductivity and redox conditions in Arabian Sea sediments. *Geochimica et Cosmochimica Acta* **69**(4), 919–931. <https://doi.org/10.1016/j.gca.2004.05.044>
- Sharma M, Mishra S, Dutta S, Banerjee S and Shukla Y (2009) On the affinity of *Chuarina-Tawuia* Complex; a multidisciplinary study. *Precambrian Research* **173**(1–4), 123–136. <https://doi.org/10.1016/j.precamres.2009.04.003>
- Sharma M, Pandey SK and Kumar S (2020) Vindhyan Basin, Son Valley Area, Central India: Field Trip Guide. New Delhi: 36th International Geological Congress (IGC). 176 pp.
- Simpson SL, Apte SC and Batley GE (1998) Effect of short-term resuspension events on trace metal speciation in polluted anoxic sediments. *Environmental Science & Technology* **32**(5), 620–625. <https://doi.org/10.1021/es970568g>
- Singh AK and Chakraborty PP (2022) Shales of Palaeo-Mesoproterozoic Vindhyan Basin, central India: insight into sedimentation dynamics of Proterozoic shelf. *Geological Magazine* **159**(2), 247–268. <https://doi.org/10.1017/S0016756820001168>
- Singh IB (1976) Depositional environment of the Upper Vindhyan sediments in the Satna–Maihar area, Madhya Pradesh and its bearing on the evolution of Vindhyan sedimentation basin. *Journal of the Palaeontological Society of India* **19**, 48–70.
- Singh VK, Babu R and Shukla M (2009) Discovery of carbonaceous remains from the Neoproterozoic shales of Vindhyan Supergroup, India. *Journal of Evolutionary Biology Research* **1**(1), 1–17. <https://doi.org/10.5897/JEBR.9000005>
- Singh VK, Babu R and Shukla M (2011) Heterolithic prokaryotes from the coated grains bearing carbonate facies of Bhandar Group, Madhya Pradesh, India. *Journal of Applied Biosciences* **37**, 80–90.
- Soni MK, Chakraborty S and Jain VK (1987) Vindhyan Supergroup: a review. *Geological Society of India Memoir* **6**, 87–138.
- Sperling EA, Knoll AH and Girguis PR (2015) The ecological physiology of Earth's second oxygen revolution. *Annual Review of Ecology, Evolution, and Systematics* **46**, 215–235. <https://doi.org/10.1146/annurev-ecolsys-110512-135808>
- Srivastava BN, Rana MS and Verma NK (1983) Geology and hydrocarbon products of the Vindhyan Basin. In *Petroliferous Basins of India* (eds LL Bhandari, BS Venkatachala, R Kumar, SN Swamy, P Garga & DC Srivastava), pp. 179–189. Dehradun, India: Petroleum Asia Journal.
- Srivastava P (2004) Carbonaceous fossils from the Panna Shale, Rewa Group (Upper Vindhyan), Central India: A possible link between evolution from micro-megascopic life. *Current Science* **86**(5), 644–646.
- Sulu-Gambari F, Hagens M, Behrends T, Seitaj D, Meysman FJ, Middelburg J and Slomp CP (2018) Phosphorus cycling and burial in sediments of a seasonally hypoxic Marine Basin. *Estuaries and coasts* **41**, 921–939. <https://doi.org/10.1007/s12237-017-0324-0>
- Sur S, Schieber J and Banerjee S (2006) Petrographic observations suggestive of microbial mats from Rampur Shale and Bijaigarh Shale, Vindhyan Basin, India. *Journal of Earth Systems Science* **115**, 61–66.
- Sweere T, van den Boorn S, Dickson AJ and Reichart GJ (2016) Definition of new trace-metal proxies for the controls on organic matter enrichment in marine sediments based on Mn, Co, Mo and Cd concentrations. *Chemical Geology* **441**, 235–245. <https://doi.org/10.1016/j.chemgeo.2016.08.028>
- Sweere TC, Dickson AJ, Jenkyns HC, Porcelli D and Henderson GM (2020) Zinc-and cadmium-isotope evidence for redox-driven perturbations to global micronutrient cycles during Oceanic Anoxic Event 2 (Late Cretaceous). *Earth and Planetary Science Letters* **546**, 116427. <https://doi.org/10.1016/j.epsl.2020.116427>
- Takahashi G (2015) Sample preparation for X-ray fluorescence analysis. *Rigaku Journal* **31**(1), 26–30.
- Tripathy GR and Singh SK (2015) Re-Os depositional age for black shales from the Kaimur Group, Upper Vindhyan, India. *Chemical Geology* **413**, 63–72.
- Twining BS and Baines SB (2013) The trace metal composition of marine phytoplankton. *Annual Review of Marine Science* **5**, 191–215. <https://doi.org/10.1146/annurev-marine-121211-172322>
- Valdiya KS (1969) Stromatolites of the lesser Himalayan carbonate formations and the Vindhyan. *Journal of the Geological Society of India* **10**(1), 1–25.
- van der Weijden CH, Reichart GJ and van Os BJ (2006) Sedimentary trace element records over the last 200 kyr from within and below the northern Arabian Sea oxygen minimum zone. *Marine Geology* **231**(1–4), 69–88. <https://doi.org/10.1016/j.margeo.2006.05.013>
- van Geen A, McCorkle DC and Klinkhammer GP (1995) Sensitivity of the phosphate-cadmium-carbon isotope relation in the ocean to cadmium removal by suboxic sediments. *Paleoceanography* **10**, 159–169. <https://doi.org/10.1029/94PA03352>
- Viehmann S, Hohl SV, Kraemer D, Bau M, Walde DH, Galer SJ, Jiang SY and Meister P (2019) Metal cycling in Mesoproterozoic microbial habitats: insights from trace elements and stable Cd isotopes in stromatolites. *Gondwana Research* **67**, 101–114. <https://doi.org/10.1016/j.gr.2018.10.014>
- Wagner M, Hendy IL, McKay JL and Pedersen TF (2013) Influence of biological productivity on silver and redox-sensitive trace metal accumulation in Southern Ocean surface sediments, Pacific sector. *Earth and Planetary Science Letters* **380**, 31–40. <https://doi.org/10.1016/j.epsl.2013.08.020>
- Wani H and Mondal M (2011) Evaluation of provenance, tectonic setting, and paleoredox conditions of the Mesoproterozoic–Neoproterozoic basins of the Bastar craton, Central Indian Shield: using petrography of sandstones and geochemistry of shales. *Lithosphere* **3**, 143–154. <https://doi.org/10.1130/L74.1>
- Wilde P, Lyons TW and Quinby-Hunt MS (2004) Organic carbon proxies in black shales: molybdenum. *Chemical Geology* **206**, 167–176. <https://doi.org/10.1016/j.chemgeo.2003.12.005>
- Wyrski K (1962) The oxygen minima in relation to ocean circulation. *Deep Sea Research and Oceanographic Abstracts* **9**(1–2), 11–23. [https://doi.org/10.1016/0011-7471\(62\)90243-7](https://doi.org/10.1016/0011-7471(62)90243-7)
- Xiang L, Schoepfer SD, Zhang H, Cao CQ and Shen SZ (2018) Evolution of primary producers and productivity across the Ediacaran–Cambrian transition. *Precambrian Research* **313**, 68–77. <https://doi.org/10.1016/j.precamres.2018.05.023>
- Xiao S and Laflamme M (2009) On the eve of animal radiation: phylogeny, ecology and evolution of the Ediacara biota. *Trends in Ecology & Evolution* **24**, 31–40. <https://doi.org/10.1016/j.tree.2008.07.015>
- Xiong Z, Li T, Algeo T, Chang F, Yin X and Xu Z (2012) Rare earth element geochemistry of laminated diatom mats from tropical West Pacific: evidence for more reducing bottom waters and higher primary productivity during the Last Glacial Maximum. *Chemical Geology* **296**, 103–118. <https://doi.org/10.1016/j.chemgeo.2011.12.012>
- Xu Y, Feng L, Jeffrey PD, Shi Y and Morel FM (2008) Structure and metal exchange in the cadmium carbonic anhydrase of marine diatoms. *Nature* **452**, 56–61. <https://doi.org/10.1038/nature06636>